Cerebral Cortex January 2014;24:119–142
doi:10.1093/cercor/bhs293
Advance Access publication October 4, 2012

Membrane Resonance Enables Stable and Robust Gamma Oscillations

Vasile V. Moca[1], Danko Nikolić[2,3,4], Wolf Singer[2,3,4] and Raul C. Mureşan[1,2]

[1]Department of Experimental and Theoretical Neuroscience, Center for Cognitive and Neural Studies (Coneural), Romanian Institute of Science and Technology, Str. Cireşilor 29, 400487 Cluj-Napoca, Romania, [2]Department of Neurophysiology, Max Planck Institute for Brain Research, Deutschordenstrasse 46, D-60528 Frankfurt/M, Germany, [3]Frankfurt Institute for Advanced Studies (FIAS), Ruth-Moufang-Strasse 1, D-60438 Frankfurt/M, Germany and [4]Ernst Strüngmann Institute (ESI) for Neuroscience in Cooperation with Max Planck Society, Deutschordenstrasse 46, D-60528 Frankfurt/M, Germany

Address Correspondence to Raul C. Mureşan, Department of Experimental and Theoretical Neuroscience, Center for Cognitive and Neural Studies (Coneural), Romanian Institute of Science and Technology, Str. Cireşilor 29, 400487 Cluj-Napoca, Romania. Email: muresan@coneural.org

Neuronal mechanisms underlying beta/gamma oscillations (20–80 Hz) are not completely understood. Here, we show that *in vivo* beta/gamma oscillations in the cat visual cortex sometimes exhibit remarkably stable frequency even when inputs fluctuate dramatically. Enhanced frequency stability is associated with stronger oscillations measured in individual units and larger power in the local field potential. Simulations of neuronal circuitry demonstrate that membrane properties of inhibitory interneurons strongly determine the characteristics of emergent oscillations. Exploration of networks containing either integrator or resonator inhibitory interneurons revealed that: (i) Resonance, as opposed to integration, promotes robust oscillations with large power and stable frequency via a mechanism called RING (Resonance INduced Gamma); resonance favors synchronization by reducing phase delays between interneurons and imposes bounds on oscillation cycle duration; (ii) Stability of frequency and robustness of the oscillation also depend on the relative timing of excitatory and inhibitory volleys within the oscillation cycle; (iii) RING can reproduce characteristics of both Pyramidal INterneuron Gamma (PING) and INterneuron Gamma (ING), transcending such classifications; (iv) In RING, robust gamma oscillations are promoted by slow but are impaired by fast inputs. Results suggest that interneuronal membrane resonance can be an important ingredient for generation of robust gamma oscillations having stable frequency.

Keywords: ING, oscillation frequency, PING, RING, visual cortex

Introduction

Neuronal oscillations in the high-beta and -gamma frequency bands (20–80 Hz) are associated with visual processing (Gray and Singer 1989; Tallon-Baudry et al. 1997), motor control (Schoffelen et al. 2005), cognitive processes (Uhlhaas and Singer 2006; Melloni et al. 2007), cortical and hippocampal dynamics (Sirota et al. 2008), and their disruption correlates with abnormal brain function (Uhlhaas and Singer 2006). Recently, the functional role of such oscillations has been questioned because of the input dependence of oscillation frequency in sensory cortices. When visual contrast is manipulated, the frequency of gamma oscillations covaries with the strength of input (Ray and Maunsell 2010). Similarly, when moving stimuli are used, oscillation frequency increases with stimulus velocity (Gray et al. 1990) and because of the anisotropy of the cortical magnification factor, stimuli of equal velocity generate oscillations with different frequencies when presented at different retinal eccentricities (Lima et al. 2011). Drifting and heterogeneous oscillation frequencies could impair synchronization of gamma oscillations, raising doubt on whether these can support binding (Singer 1999) or communication by coherence (Fries 2005). Because gamma oscillations are expressed differently under different conditions and are modulated by several factors, there is still a poor understanding of their implication in various brain processes. Arguably, the properties and possible functional role of gamma oscillations could be better understood if more details are revealed about underlying mechanisms.

The mechanisms leading to beta/gamma oscillations are not entirely clear (Tiesinga and Sejnowski 2009), but it is generally accepted that they rely on push–pull interplay between excitation and inhibition (Buzsáki and Wang 2012). This can be mediated either by coupled populations of excitatory and inhibitory neurons (Hansel and Mato 2003), called Pyramidal INterneuron Gamma (PING) mechanism (Börgers and Kopell 2003), or by tonic excitation of reciprocally coupled inhibitory neurons, called INterneuron Gamma (ING) mechanism (Whittington et al. 2000), in which case gamma oscillations can arise also in purely inhibitory networks (Wang and Buzsáki 1996; Brunel and Hakim 1999). A consensus regarding the prevalence of PING or ING has not yet been reached (Tiesinga and Sejnowski 2009), but it is likely that both may be at work in different brain systems, during different brain states, and under the influence of different neuromodulators (Whittington et al. 1995; Buhl et al. 1998; Fisahn et al. 1998). Nevertheless, it is now clearly recognized that inhibition plays a crucial role in emergence of fast oscillations (Whittington et al. 2000) and it has been demonstrated that parvalbumin expressing fast-spiking (FS) GABA-ergic interneurons play a causal role in supporting gamma oscillations (Buzsáki et al. 1983; Bragin et al. 1995; Hasenstaub et al. 2005; Cardin et al. 2009; Sohal et al. 2009).

Another important mechanism related to oscillations is the intrinsic frequency preference of neurons (Llinás et al. 1991; Gray and McCormick 1996; Hutcheon and Yarom 2000), also called membrane resonance (Izhikevich 2007; Mureşan and Savin 2007) that can naturally support rhythms. For example, membrane resonance in hippocampal pyramidal neurons (Leung and Yu 1998; Leung and Yim 1991), manifest in the theta frequency band, was shown to contribute to development of theta oscillations in models of CA3 (Tiesinga et al. 2001). Membrane resonance was studied relatively seldom in the context of fast oscillations, in spite of the fact that inhibitory interneurons, especially of parvalbumin expressing FS type, can exhibit frequency preference, usually in the beta/gamma

bands (20–80 Hz) (Pike et al. 2000; Fellous et al. 2001; Bracci et al. 2003). So far, it is not clear how membrane properties of inhibitory interneurons may complement or interact with the widely accepted push–pull emergence mechanism of fast network oscillations, nor is it clear which properties of such oscillations may be influenced by resonance.

Here, we first show that *in vivo* gamma oscillations in the cat visual cortex can sometimes exhibit remarkably stable oscillation frequency and most likely emerge from a PING-like mechanism. Based on *in vivo* findings, we further use computational modeling to establish how the observed properties of beta/gamma oscillations are determined by membrane properties of inhibitory interneurons, with a focus on the stability of oscillation frequency when the input fluctuates. Throughout the rest of this paper, we will use the term *gamma oscillation* to refer to a broad frequency band of 20–80 Hz, because there is evidence that high-beta (20–30 Hz) and gamma (30–80 Hz) frequency bands are not clearly separated, but seem to be generated by the same underlying process (Steriade 2006).

Materials and Methods

Ethics Statement

Experimental data were recorded from anesthetized and paralyzed adult cats, bred in the facilities of the Max-Planck Institute for Brain Research. All the experiments were conducted in accordance with the European Communities Council Directive of 24 November 1986 (86/609/EEC), according to the guidelines of the Society for Neuroscience and the German law for the protection of animals, approved by the local government's ethics committee and overseen by a veterinarian.

Experimental Procedures and Recording

Anesthesia was induced with ketamine (Ketanest, Parke–Davis, 10 mg kg^{-1}, intramuscular) and xylazine (Rompun, Bayer, 2 mg kg^{-1}, intramuscular) and maintained with a mixture of 70% N_2O and 30% O_2 supplemented with halothane (0.5–1.0%). After tracheotomy, animals were placed in a stereotactic frame. A craniotomy was performed, and the skull was cemented to a metal rod. After completion of all surgical procedures, the ear and eye bars were removed, and the halothane level was reduced to 0.4–0.6%. After assuring that the level of anesthesia was stable and sufficiently deep to prevent any vegetative reactions to somatic stimulation, animals were paralyzed with pancuronium bromide (Pancuronium, Organon, 0.15 mg kg^{-1} h^{-1}). The end-tidal CO_2 and rectal temperature were kept in the range of 3–4% and 37–38 °C, respectively. Stimuli were presented binocularly on a 21-inch computer screen (HITACHI CM813ET) with 100 Hz refresh rate. To obtain binocular fusion, the optical axes of the two eyes were first determined by mapping the borders of the respective receptive fields and then aligned on the computer screen with adjustable prisms placed in front of one eye. Visual stimulation was achieved through ActiveSTIM (www.ActiveSTIM.com). Data were recorded from area 17 of 2 adult cats by inserting multiple silicon-based multi-electrode probes (16 channels per probe) supplied by the Center for Neural Communication Technology at the University of Michigan (Michigan probes). Each probe consisted of four 3 mm long shanks that were separated by 200 µm (inter-shank distance) and contained four electrode contacts each (1250 μm^2 area, 0.3–0.5 MΩ impedance at 1000 Hz, inter-contact distance 200 µm). Signals were amplified 10 000× and filtered between 500 Hz and 3.5 kHz and between 1 and 100 Hz for extracting spiking activity and local-field potentials (LFPs), respectively. Waveforms of detected spikes were recorded for a duration of 1.2 ms, which allowed the later application of offline spike-sorting techniques to extract single units (SUs).

Stimuli

Center-surround Grating Stimuli

Sinusoidal gratings of three different sizes (small, medium, and large) and two orientations (horizontal and vertical) were presented individually or superimposed. Gratings spanned visual angles of 7°, 14°, and 21°, had a spatial frequency of 1° per grating cycle, and were drifted at a speed of 1.5° per second, orthogonal to their orientation and in one direction only. Stimuli included 6 individual gratings, 4 superimposed gratings with a small central grating surrounded by an orthogonal medium or large grating, and 4 superimposed gratings consisting of a small grating separated by a gray ring (3.5° wide) from a surrounding large grating of identical or orthogonal orientation. The resulting 14 stimuli were randomly presented 20 times each, leading to a total number of 280 trials. Trials were 6000 ms long with the stimulus presented between 1000 and 5000 ms. These stimuli were used to record from Cat 1, with 85 SUs isolated off-line.

Drifting Sinusoidal Grating Stimuli

Sinusoidal gratings moving in 12 directions in steps of 30° were presented in trials of 4800 ms duration (1000 ms spontaneous activity, 3500 ms stimulus, 300 ms stimulus-OFF response). Gratings spanned 12° of visual angle, had a spatial frequency of 2.4° per cycle, and drifted with a speed of 2° per second. Each direction was presented 20 times in a randomized order leading to the total of 240 presentations (trials). These stimuli were used to record data from Cat 2 (39 SUs).

Estimation of Oscillation Strength and Oscillation Frequency

The oscillation strength and frequency of the activity of single cells were estimated by using the oscillation score (OS) (Mureşan et al. 2008). The OS relies on the autocorrelation histogram (ACH) computed over all presentations of the corresponding stimulus. The central peak of the ACH is then removed and the fast Fourier transform (FFT) of the peakless ACH is computed. We used an ACH of ±256 ms (512 bins), yielding an FFT bin of ~2 Hz (the sampling frequency for spike-trains was 1000 Hz). Therefore, the precision of the oscillation frequency estimate was ±1 Hz. After computing the FFT, a peak was identified in the frequency band of interest, and the OS was defined as the size of the peak relative to the average (baseline) of the FFT spectrum. The oscillation frequency corresponded to the location of the peak in the analyzed frequency band. To avoid false estimates of frequency due to harmonics or overestimation of OS due to data with very low spike rate, ACHs and their corresponding frequency spectra were frequently inspected visually—see (Mureşan et al. 2008).

It is recommended to compute the OS in a narrow band of interest, usually not exceeding one biological frequency band (Mureşan et al. 2008). Here, we computed the OS in a broad band spanning both high-beta and gamma (20–80 Hz) for the sake of covering the entire relevant frequency range. Analyses were, however, repeated also in a narrow band, between 20–40 Hz, around the oscillation frequency observed in the recorded data (28.83 ± 1.66 Hz). The broad and the narrow band OS analyses yielded similar results.

Sliding Window Analysis of Experimental Data (Stability Test)

To determine the stability of the oscillation frequency and firing rate, we conducted a sliding-window analysis of spike trains by computing the instantaneous oscillation frequency and instantaneous firing rate along the presentation of a stimulus, and estimating the fluctuations of the two. Data were collected from 2 cats and out of a total of 124 SUs isolated through off-line spike sorting, 79 showed oscillatory responses. However, only 62 out of these 79 oscillating cells produced enough spikes to allow for the estimation of OS in at least 20 overlapping windows of 500 ms length (see below). There were no other selection criteria for including a cell into analysis: We included not only cells whose responses were modulated strongly by the passage of the grating stripes over the receptive fields (i.e. simple cells) but also those with weak modulation (complex cells) (Hubel and Wiesel 1962).

A sliding window of 500 ms was moved in steps of 10 ms over the sustained part of the responses (200 ms following stimulus onset until the end of stimulation). Not all windows were used in the analysis but only those for which an oscillation frequency could be measured. Because the windows were relatively short and the firing rate of cortical neurons was low, there were only few spikes to estimate oscillatory patterning and this made estimation of oscillation frequency very difficult. For very low rates, the OS tends to be overestimated (Mureşan et al. 2008) and for that reason, when establishing if the activity in a window was oscillatory or not, we imposed thresholds also on the number of action potentials in the window. A window was considered to exhibit oscillatory activity if the OS in the 20–80 Hz band ≥7, and the window had sufficient number of action potentials to produce an ACH with ≥0.07 coincidences/ACH-bin (weak oscillations, conservative rate threshold), or if the OS in the 20–80 Hz band was ≥10 and the baseline of the ACH exceeded 0.025 coincidences/ACH-bin (stronger oscillations, relaxed rate threshold). An analysis with the frequency band restricted to 20–40 Hz yielded identical results (not shown). Out of the total 108 980 windows, 56 525 (51.87%) were included in the analysis. For the comparison, firing rates were always computed for the same windows used for calculation of the oscillation frequency.

For the 62 selected units (42 and 20 units for Cat 1 and Cat 2, respectively), we investigated the fluctuation of oscillation frequency and firing rate along the stimulus for at least 1 and up to 14 (on average 5.5) different stimuli, that is, for cases where the oscillatory response could be measured. This led to a total of 341 tests of stability, with 270 and 71 tests for Cat 1 and Cat 2, respectively. For each test, we computed the standard deviation and coefficient of variation of the oscillation frequency and firing rate across the corresponding sliding windows (on average 161.99 windows for each test). The standard deviation of the oscillation frequency was termed "frequency drift".

Analysis of Putative Excitatory/Inhibitory Neurons' Firing Sequence

To attempt to separate putative pyramidal neurons (wider spike) from putative interneurons (more narrow spike) (González-Burgos et al. 2005; Mitchell et al. 2007), action potential width was quantified as the time interval between the two extremes of the extracellular voltage (Supplementary Fig. S1A). This method is different from previously reported measures of spike width where the beginning and end of an action potential were defined as the moments at which the excursion of the voltage was below a certain threshold [e.g. 10% of the first and second peak, respectively; (González-Burgos et al. 2005)]. Neurons in the cat visual cortex frequently exhibit strong bursting during epochs with oscillatory activity in the gamma band, and this makes it difficult to use such methods to detect the beginning and end of the spike with sufficient precision. We found that measuring the time interval between the two extremes of the extracellular voltage was more robust, as has been also described previously (Mitchell et al. 2007). Data were carefully spike-sorted again, only the cells with clearly identifiable spike shape being selected (22 cells for Cat 1 and 14 cells for Cat 2).

After computing the width of individual action potentials, we considered, for each animal and each stimulus, only pairs of cells that exhibited oscillatory activity and were synchronized to make sure they participated in the same oscillatory process. Thus, we included in the analysis only cells that had OS >8 and where the central peak of their cross-correlation histogram (CCH) was at least 2× larger than the baseline of the CCH. The delay between a pair of cells was inferred from the offset of the central peak of the CCH relative to zero (Supplementary Fig. S1B).

Because of the constraints regarding oscillatory activity and synchronization of pairs of cells whose activity has to be recorded simultaneously, we could not pool data across different sessions and animals as was the case in other studies (Mitchell et al. 2007). Therefore, only a limited number of cells matched all criteria for inclusion in the analysis. We could not find clear clusters based on action potential width that would identify the two different groups of principal cells and interneurons. Rather, action potential width was distributed in a continuum across the included cells, as was reported also in other studies (González-Burgos et al. 2005; Krimer et al. 2005). The lack of clear clustering of action potential widths could be due to filtering (Henze et al. 2000; Constantinidis and Goldman-Rakic 2002; Mitchell et al. 2007) and/or the spike-sorting procedure (Mitchell et al. 2007). In cat area 17 identification of inhibitory interneurons was difficult both because extracellular recording electrodes might seldom pick up their weaker spikes and because these spikes may be mixed with others from pyramidal cells and cannot be clearly separated during spike sorting. As a result, it is possible that waveforms extracted by spike sorting are a mix of pyramidal and interneuronal waveforms, yielding a continuum distribution of action potential widths (Mitchell et al. 2007). For these reasons, we developed a "smooth" method to get a hint on the likely firing sequence of putative pyramidal neurons and interneurons: We correlated the CCH delay with the difference between the widths of the action potential of the corresponding cells in each pair (Supplementary Fig. S1C). When wider action potentials precede narrower ones, the correlation is positive.

Network Architecture and Connectivity

Simulated networks were built on a square grid with an edge length $L = 25$ units, resulting in $25 \times 25 = 625$ neurons. Each unit was either excitatory or inhibitory and their proportion in the network was 80% excitatory and 20% inhibitory (Supplementary Fig. S2A). Excitatory and inhibitory neurons were distributed randomly on the grid. All neurons belonging to one of the two populations had identical parameters, connectivity parameters, and input statistics. We chose small-world connectivity between neurons because it matches best the connection patterns in brain circuits, both in terms of anatomical (Sporns et al. 2004) and functional connectivity (Yu et al. 2008). We have observed a small advantage in obtaining robust oscillations when using a small-world topology when compared with a random one, but the connectivity factor was not investigated systematically in the present study. Nevertheless, results reported with the small-world architecture were reproduced also with randomly connected networks (not shown). Network connectivity was governed by the rules summarized in Supplementary Figure S2B, and as follows: For each postsynaptic neuron, a set of eligible presynaptic neurons was chosen from its vicinity. This vicinity circle was centered on the postsynaptic (target) neuron and was defined by a radius, r, expressed relative to the largest distance possible on the grid (diagonal). Inhibitory neurons received more local inputs ($r_I = 0.2$) than excitatory neurons ($r_E = 0.3$). To eliminate border effects, the grid had a periodic boundary condition (was wrapped around the edges). From the neurons that laid within the vicinity circle, a set of presynaptic neurons were chosen based on the local connection probability, P. Local connection probabilities were chosen for excitatory, $P_E = 0.3$, and inhibitory targets, $P_I = 0.65$, such that the number of connections per target remained about the same, counterbalancing for the differences in r. No autaptic (self) connection was allowed. To create small-world topology, some of the connections were replaced with long-range connections to neurons outside the vicinity circle. This rewiring probability was the same for all the neurons ($P_{EI} = 0.2$ and $P_{II} = 0.2$). The wiring pattern described above took into consideration that parvalbumin-expressing inhibitory interneurons, known to be involved in gamma oscillations, are generally contacting proximal pyramidal cells, but can also have more long-range connections (Thomson and Bannister 2003). Based on anatomical evidence, we considered that excitatory local connections spanned a larger territory compared with the local inhibitory connections and in addition that both the inhibitory and excitatory populations can contact more distal targets, i.e. corresponding to cortico-cortical connectivity (Thomson and Bannister 2003). On average, excitatory neurons were contacted by ~58 presynaptic neurons, while inhibitory neurons were contacted by ~45 presynaptic neurons.

Neuron Types

Excitatory neurons were always of the leaky integrate-and-fire (IF) type with membrane resistance $R_m = 20$ MΩ and membrane capacitance $C_m = 1$ nF (time constant of 20 ms) (see Table 1, E_IF). In the simulations with purely integrator networks, inhibitory interneurons were of the same type (leaky IF) and had $R_m = 10$ MΩ and membrane capacitance $C_m = 1$ nF (time constant of 10 ms) (see Table 1, I_IF). For integrator–resonator networks, the inhibitory IF neurons were replaced with Izhikevich-type resonators (Izhikevich 2003) (see Table 1, I_RES):

$$\begin{aligned} \dot{u} &= 0.04u^2 + 5u + 140 - r + I \\ \dot{r} &= a(bu - r) \\ \text{if } u \geq 30, \text{ then } &\begin{cases} u \leftarrow c \\ r \leftarrow r + d \end{cases} \end{aligned} \tag{1}$$

where u is the membrane potential, r is a recovery variable, I is the input current, and a, b, c, d are parameters (set to $a = 0.1$, $b = 0.26$, $c = -62.5$, and $d = 2$ for resonators).

Parameter c (resting potential) was set to −62.5 mV (−65 mV in the original Izhikevich model) because the neuron maintains this stable voltage in the absence of any external input. These resonator neurons have frequency preference, the input impedance exhibiting a peak centered around 22–24 Hz (Supplementary Fig. S3B).

To test for the model independence of observed phenomena, in some simulations we used another model for resonator interneurons, i.e. the resonate-and-fire model (RF) (Izhikevich 2001) (Table 1, I_RF). The original RF model was modified by introducing a membrane potential variable that ranges between a resting voltage of −65 mV and a firing threshold of −45 mV, and a refractoriness kernel:

$$\begin{aligned} \omega &= 2\pi f_{res} \\ \dot{x} &= bx - \omega y + I \\ \dot{y} &= \omega x + by \\ \dot{r} &= -\tau_{ref} r \\ u &= -65 + 20y - r \end{aligned} \tag{2}$$

where x and y are dynamics variables from the original RF model (Izhikevich 2001), I is the input current, b represents the rate of attraction to rest (<0), f_{res} is the resonance frequency of the neuron, r is an exponentially decaying (with decay constant τ_{ref}) refractoriness kernel introduced after the spike, and u is the membrane potential.

When the membrane potential u exceeds the threshold of −45 mV, the neuron fires a spike, and variables are reset as follows:

$$\begin{aligned} x &\leftarrow 0 \\ y &\leftarrow 1 \\ r &\leftarrow r + 40 \end{aligned} \tag{3}$$

Table 1.
Parameters of neuron models

	Parameter name	Value
E_IF	R_m (MΩ)	20
	C_m (nF)	1
	U_{rest} (mV)	−65
	U_{reset} (mV)	−65
	Threshold (mV)	−45
I_IF	R_m (MΩ)	10
	C_m (nF)	1
	U_{rest} (mV)	−65
	Threshold (mV)	−45
I_RES	a	0.1
	b	0.26
	c	−62.5
	d	2
I_RF	f_{res}	Between 20–40 Hz, depending on setup
	b	−30
	τ_{ref}	5 ms

such that the membrane is hyperpolarized at −85 mV after spike but the internal variables x and y continue to evolve on the dampened resonant oscillation curve. The refractoriness kernel ensures a realistic dynamics for both the membrane and the postsynaptic currents (dependent on the postsynaptic membrane potential) of the modified RF neuron.

Importantly, RF neurons exhibit resonance at a frequency that is explicitly defined in the model (parameter f_{res}), rendering them feasible to study networks with arbitrary interneuronal resonant frequency. Unlike RES neurons, the impedance profile of RF neurons is not voltage dependent (Supplementary Fig. S3C), as is also the case with IF neurons.

Synapses

Four types of synapses connect all possible four combinations of excitatory and inhibitory pre- and postsynaptic neurons. According to Dale's law, excitatory neurons were allowed to form only excitatory connections with postsynaptic targets and inhibitory neurons only inhibitory connections. Both types of neurons received both excitatory and inhibitory synaptic input. Below, the type of synapse is codified by two letters. The first letter corresponds to the type of presynaptic neuron and thus to the type of the synapses, and the second letter corresponds to the type of the target neuron. All synapses were conductance-based (postsynaptic currents depend on reversal potential and the postsynaptic membrane potential), with an exponential decay constant of 3 ms for excitatory synapses (EE, EI), which corresponds to AMPA synapses, and 5 ms for inhibitory synapses (IE, II), which corresponds to $GABA_A$ synapses. In some simulations, the time constants of inhibitory synapses were manipulated systematically between 1 and 11 ms. The amplitudes (weights) of the synapses were randomly selected from the interval [0, *maxSyAmp*], where *maxSyAmp* depended on the type of the synapse (Table 2) and was set such that networks had realistically low firing rates, matching *in vivo* findings (Olshausen and Field 2006). The *maxSyAmp* variable was scaled independently for excitatory and inhibitory synapses in the simulations that manipulated the strength of connectivity.

Each synapse had in addition a conduction delay proportional to the distance between the pre- and postsynaptic neuron. The minimum delay was 0.1 ms and, unless specified otherwise, the delay between the two most distant neurons was 3 ms. The latter value was an upper bound on local circuit conduction delays in the cortex (Sabatini and Regehr 1999).

Simulations were carried out with the Neocortex environment (Mureşan and Ignat 2004) using an integration time step of 0.1 ms. For additional details on the shape of synaptic currents and simulation, see Mureşan and Ignat (2004) and Mureşan and Savin (2007).

External Drive

Each neuron received two types of inputs. The first input was a sinusoidal current, corresponding to an external stimulation similar to a grating passing trough the receptive field of a simple cell. The sinusoidal input was shifted such as to prevent negative values (not centered on 0, but with an offset equal to the amplitude of the sine function) and was present between stimulus onset, at 1000 ms, and stimulus offset, at 5000 ms, in trials lasting 6000 ms. Amplitudes of this input depended on the simulation and the type of neuron: both the excitatory and inhibitory populations received input (Table 2). The frequency of the sine was 0.5 Hz if not otherwise specified. Each stimulation epoch was repeated 20 times, yielding 20 trials. In some simulations, we also used constant currents instead of sinusoidal inputs (this was always specified).

The second type of input modeled the spontaneous release of miniature synaptic potentials—minis (Paré et al. 1997; Paré et al. 1998). Minis were modeled as exponentially decaying synaptic conductances released with a given probability (0.09/ms for glutamate and 0.02/ms for GABA) similarly as reported in Mureşan and Savin (2007). Glutamate minis had a decay time constant of 3 ms, while GABA minis had 5 ms. Similarly to the case of synapses, the amplitudes of minis were randomly selected from an interval between 0 and a maximum value. With this maximum value, the level of spontaneous activity in the

Table 2.
Simulation and network parameters

Category	Parameter name	IF–IF	IF–RES	IF–RF
Simulation	Number of trials		20	
	Trial duration (ms)		6000	
	Integration step (ms)		0.1	
	Stim. On (ms)		1000	
	Stim. Off (ms)		5000	
Network	Lattice size		25 × 25 (625 neurons)	
	Percentage of E neurons		80%	
	Percentage of I neurons		20%	
Connectivity	P_E		0.3	
	P_I		0.65	
	r_E		0.3	
	r_I		0.2	
	P_{EI}		0.2	
	P_{II}		0.2	
Neuron types	E neuron		E_IF	
	I neuron	I_IF	I_RES	I_RF
Synapses	Maximum delay (ms)		3	
	EE reversal potential (mV)		0	
	EI reversal potential (mV)		0	
	IE reversal potential (mV)		−90	
	II reversal potential (mV)		−90	
	EE *maxSyAmp*	0.022	0.011	0.022
	EI *maxSyAmp*	0.022	0.011	0.0065
	IE *maxSyAmp*	0.2	0.2	0.15
	II *maxSyAmp*	0.0275	0.035	0.01
	EE decay constant (ms)		3	
	EI decay constant (ms)		3	
	IE decay constant (ms)		5	
	II decay constant (ms)		5	
MINIs	Glutamate to E neurons scaling		0.0625	
	Glutamate to I neurons scaling	0.09	0.00719	0.0035
	GABA to E neurons scaling		0.04	
	GABA to I neurons scaling	0.04	0.0049	0.00224
	Glutamate to E neurons decay constant (ms)		3	
	Glutamate to I neurons decay constant (ms)		3	
	GABA to E neurons decay constant (ms)		5	
	GABA to I neurons decay constant (ms)		5	
	Glutamate MINIs release probability		0.09	
	GABA MINIs release probability		0.02	
Input current	Sine frequency (Hz)		0.5	
	Sine amplitude to E neurons (nA)		1	
	Sine amplitude to I neurons (nA)	0.465	0.07	0.034
	Sine offset to E neurons (nA)		1	
	Sine offset to I neurons (nA)	0.465	0.07	0.034

network was regulated. Amplitudes of minis are given in Table 2. Both synapses and mini amplitudes had to be scaled differently for IF, RES, and RF populations due to the different excitability of these models (Mureşan and Savin 2007) (see Table 2).

Calibration of Reference Networks

To make sure that IF–IF, IF–RES, and IF–RF networks are in the same operating regime, we first calibrated the parameters for reference networks. Calibration started by considering IF–IF, IF–RES, and IF–RF networks that had identical connectivity, differing only in the type of interneuron. We first silenced the sinusoidal input and set all synaptic strengths to zero, yielding only uncoupled populations of neurons driven by minis. Amplitudes of minis were tuned such that corresponding populations of excitatory and inhibitory neurons had the same spontaneous firing rates in all types of networks. Sinusoidal input to inhibitory neurons had to be different for IF, RES, and RF interneurons because of differences in excitability of these models (Mureşan and Savin 2007), and was set such as to obtain the same average firing rate of interneurons in all networks. Input to excitatory neurons was the same in all networks because the excitatory population was identical. Synaptic connections were then added and tuned until excitatory and inhibitory populations exhibited firing rates consistent to those observed in the data.

Analyses of Network Activity

All quantitative results were computed by setting up at least 10 different networks of each type. The wiring of each network was done according to the wiring principles described above, but actual connections were created randomly with the probabilities and rules specified before. Thus, each instantiation created a slightly different network and therefore, in order to obtain robust estimates, we computed all quantitative results by presenting the input 20 times to each network, and then averaging across networks. In all cases, the standard deviation was also computed, in order to get an estimate of variability.

Synchronization Index

To quantify the synchronization of a population of neurons, we developed a measure called *Synchronization Index* (SI). The measure first computes the time resolved (unnormalized) population rate by computing the spike count across all neurons in bins of 1 ms along the trial. To identify oscillation cycles more precisely, this population rate is smoothed with a Gaussian kernel having SD = 5 ms and the local maxima (peaks) and their neighboring local minima (troughs) of the smoothed population rate are identified. When networks are engaged into coherent oscillations, these local maxima and minima occur periodically, being located at each oscillation cycle. For each oscillation cycle, identified as the period between two consecutive troughs, the corresponding piece of the unsmoothed population rate signal reflects exactly the distribution of spikes within the cycle. The SI corresponding to the cycle is then defined as the duration of the cycle divided by the average absolute deviation of the cycle spike distribution around its median. When neurons in the population fire in synchrony, spikes are concentrated in a narrow region of the cycle, yielding low absolute deviation and a high SI. At the other extreme, when neurons are poorly synchronized, firing randomly and uniformly in the local cycle window, their absolute deviation is high and SI has low values. Thus, SI represents a measure of spread of spikes in relation to the duration of the cycle. It is independent of oscillation frequency and of firing rate.

Results

Stable Gamma Oscillations in Cat Visual Cortex

Stimulus-selective gamma oscillations, reported in the visual cortex of cats (Gray and Singer 1989), may exhibit an oscillation frequency that is stable within a few Hz, even when the firing rate of cells strongly fluctuates during the response to the stimulus. In Figure 1*A*, we show the activity of an example cell from cat area 17 in response to 20 stimulus presentations (trials) of a drifting sinusoidal grating. The ACHs computed for four non-overlapping, 500 ms long, epochs along the trial (Fig. 1*A*, top) revealed a stable oscillation frequency (~27.5 Hz), although the firing rate fluctuated strongly, as shown by the peri-stimulus time histogram (PSTH; Fig. 1*A*, bottom).

These results were consistent across all 62 investigated cells (from two different animals) that exhibited measurable gamma oscillation. For each cell that exhibited oscillatory responses to a given stimulus, a stability test for oscillation frequency and firing rate was carried out using a 500 ms sliding window along the presentation of the stimulus (see Materials and Methods). We computed the coefficients of variation (CV) of the oscillation frequency and firing rate across the corresponding windows for each stability test, thus quantifying the drift relative to the mean of oscillation frequency and firing rate along stimulus presentation. The CV of oscillation frequency was considerably smaller than the CV of firing rate, for all stability tests and in two different animals, this property being most prominent for the first animal

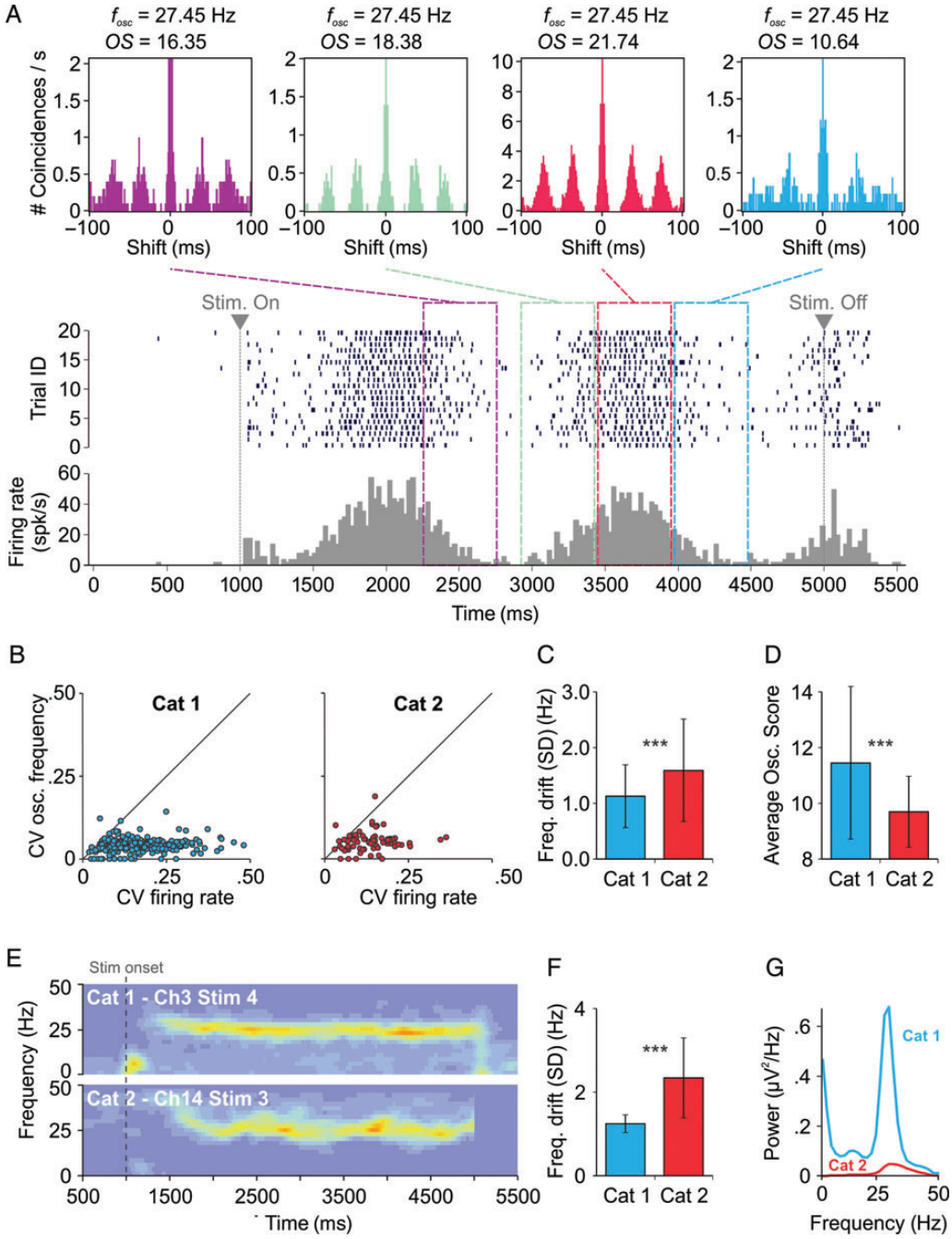

Figure 1. Gamma oscillations in individual cells of the cat visual cortex. (*A*) The firing of a "simple" cell: Top, ACHs computed at different epochs; middle, spike raster across 20 trials; bottom, peri-stimulus time histogram (PSTH). Above each ACH, the oscillation frequency (f_{osc}) and OS are indicated. Oscillation frequency was computed with a precision of ±1 Hz due to a spectral bin size of 2 Hz. (*B*) Coefficient of variation of oscillation frequency versus coefficient of variation of firing rate. (*C*) Drift of oscillation frequency (SD) along the stimulus, measured from spike trains. (*D*) OS in the 20–80 Hz band, averaged across sliding windows, cells, and stimulation conditions. (*E*) Time resolved power spectra of LFP along stimulus presentation. (*F*) Drift of oscillation frequency (SD) along the stimulus, measured from LFP. (*G*) Power spectral density of LFP averaged across electrodes and stimuli. Error bars indicate SD. ***$P < 0.001$.

(Fig. 1*B*). The standard deviation (SD) of oscillation frequency fluctuations along the stimulus (frequency drift) was on average <1.6 Hz and was significantly lower for the first animal than for the second ($P < 0.001$; Fig. 1*C*). In addition, the activity of neurons recorded in the first animal displayed a significantly stronger gamma oscillation than in the second animal ($P < 0.001$), as revealed by OSs estimated from spiking activity (Fig. 1*D*).

In an analysis of LFPs similar to that performed on individual neurons' spikes, we quantified the drift of the oscillation frequency along the stimulus by first computing the time-resolved power spectrum (Fig. 1*E*). Again, oscillation frequency appeared very stable in the first animal, with increased power at moments where the firing rate was highest (compare to Fig. 1*A*), and was somewhat more fluctuating for the second animal. For each time bin, the frequency with

maximum power was subsequently considered to be the central oscillation frequency. The frequency drift along the stimulus was then estimated as the SD of the central frequency across time bins. The frequency drift across all stimuli and electrodes was significantly smaller in the first animal than in the second ($P < 0.001$; Fig. 1*F*). Gamma power was much larger in the first animal when compared with the second (Fig. 1*G*), supporting the idea that more stable oscillations are associated with a larger power in the gamma band.

To investigate the mechanism underlying the observed gamma oscillations, we attempted to identify the firing sequence of putative excitatory pyramidal neurons and inhibitory interneurons based on the observation that FS interneurons emit narrower action potentials than non-FS neurons (González-Burgos et al. 2005). We developed a "smooth" analysis method to estimate the relation between firing sequence (delay) and action potential width in pairs of cells exhibiting synchronized oscillations (see Materials and Methods). The delay between the firing of cells correlated positively with the difference between the widths of their spikes (Supplementary Fig. S1C), for both animals (average correlations across stimuli for Cat 1 and Cat 2 were 0.65 and 0.64, respectively). The positive correlation indicates that cells with wider spikes tend to fire earlier in the gamma cycle than cells with narrower spikes, i.e. firing of putative pyramidal neurons precedes that of putative interneurons. In addition, measured delays were small (<5 ms), suggesting that inhibition followed excitation at an early phase within the gamma cycle (the oscillation period was >25 ms in our data).

Taken together, these findings indicate that gamma oscillations can be highly stable in frequency even when cortical inputs and firing rates of cells fluctuate strongly. Such stability is manifested both at the level of oscillatory activity of single cells and at the level of LFPs. In our data, larger OSs in spiking activity and larger gamma power measured in the LFP were associated with significantly more stable oscillations across two different animals. Results also suggest a PING-like emergence mechanism for the observed *in vivo* gamma oscillations (Whittington et al. 2000), where excitatory volleys rapidly entrain interneurons whose firing generates inhibition that quenches activity until the next oscillation cycle (Fisahn et al. 1998). In addition, gamma oscillations were strongly dependent on cortical state. The session recorded in the first animal was preceded by several sessions, recorded hours before, where the same stimuli did not evoke oscillatory responses, suggesting that gamma generators may dramatically change their properties as a function of cortical state.

Among many possibilities, here we investigate membrane resonance of FS interneurons (Pike et al. 2000; Fellous et al. 2001; Bracci et al. 2003) as a candidate mechanism that could flexibly change the oscillatory properties of gamma generators. FS membrane resonance is a good candidate because FS interneurons are crucially involved in the generation of gamma rhythms (Buzsáki et al. 1983; Bragin et al. 1995; Hasenstaub et al. 2005; Cardin et al. 2009; Sohal et al. 2009). Furthermore, membrane resonance can be regulated by voltage (Hutcheon et al. 1996) and neuromodulators (Steriade et al. 1991; Hutcheon et al. 1996), both of which are modulated during cortical-state changes. We next performed computer modeling of neuronal circuits, to investigate whether and how interneuronal membrane resonance could be related to the observed properties of the recorded data.

Integration and Resonance in Interneurons of Gamma Generator Circuits

Gamma generator circuits were modeled as networks with 80% excitatory and 20% inhibitory neurons, disposed on a two-dimensional lattice (Supplementary Fig. S2A). Neurons were connected via realistic conductance-based synapses in a small-world topology (Supplementary Fig. S2B). Unless otherwise specified, a distance-dependent synaptic delay was introduced (3 ms between most distant neurons), endowing the network with a realistic connectivity regime for a local circuit (Hirsch and Gilbert 1991; Lin and Faber 2002).

Excitatory neurons were always of the IF type, with membrane time constants of 20 ms, having low-pass membrane properties similar to those of pyramidal neurons (Fellous et al. 2001; Erchova et al. 2004). Inhibitory interneurons were modeled either as IF neurons, with time constants of 10 ms (González-Burgos et al. 2005), or as Izhikevich-type resonators (RES) (Izhikevich 2003). IF neurons behave as pure "integrators" (i.e. low-pass filters) and thus, do not exhibit frequency preferences in the beta/gamma range (Supplementary Fig. S3A). By contrast, RES neurons exhibit voltage-dependent membrane resonance (Hutcheon and Yarom 2000; Izhikevich 2003) having a maximal input impedance at their preferred frequency, around 22–24 Hz (Mureşan and Savin 2007) (Supplementary Fig. S3B). Depending on the type of inhibitory interneurons, we obtained two types of networks: IF–IF (excitatory IF–inhibitory IF) and IF–RES (excitatory IF–inhibitory RES). These networks were always identical in terms of excitatory neurons and the statistics of connectivity patterns but had different types of inhibitory interneurons (IF and RES, respectively). In the following simulations, we determined the way in which membrane properties of inhibitory interneurons affect emergent gamma oscillations.

Networks were driven with a sinusoidal input (Fig. 2*A*), as elicited by a sinusoidal grating in layer 4 of cat visual cortex (Fig. 1*A*). IF–IF and IF–RES networks were first calibrated (see Materials and Methods) to exhibit firing rates matching the properties of recorded data (average firing rate over the stimulation period ~4.5–4.7 spk/s), and both were able to produce gamma oscillations with a mean frequency of ~27 Hz (Fig. 2*A*–*C*). During the stimulation period (1000–5000 ms; Fig. 2*A*), average firing rates of inhibitory neurons (~11–12 spk/s) were >3-fold larger than those of excitatory neurons (~3.5–4 spk/s), matching experimental evidence (Whittington et al. 2000; Bartos et al. 2007). As a consequence, excitatory neurons skipped the majority of oscillation cycles (Nikolić 2009), whereas inhibitory neurons fired on almost every cycle (Bartos et al. 2007; Hájos and Paulsen 2009) (Supplementary Fig. S4).

Both IF–IF and IF–RES networks showed evidence of a PING-like oscillation mechanism, with inhibitory interneurons firing within the oscillation cycle at short latencies after the excitatory volley (Fig. 2*B* and *C*, top). We computed the LFP corresponding to each network by averaging the deviation of membrane potential from rest across all cells. Already from spike rasters (Fig. 2*B* and *C*, top) and LFP traces (Fig. 2*B* and *C*, middle), it was apparent that synchronization was less robust in

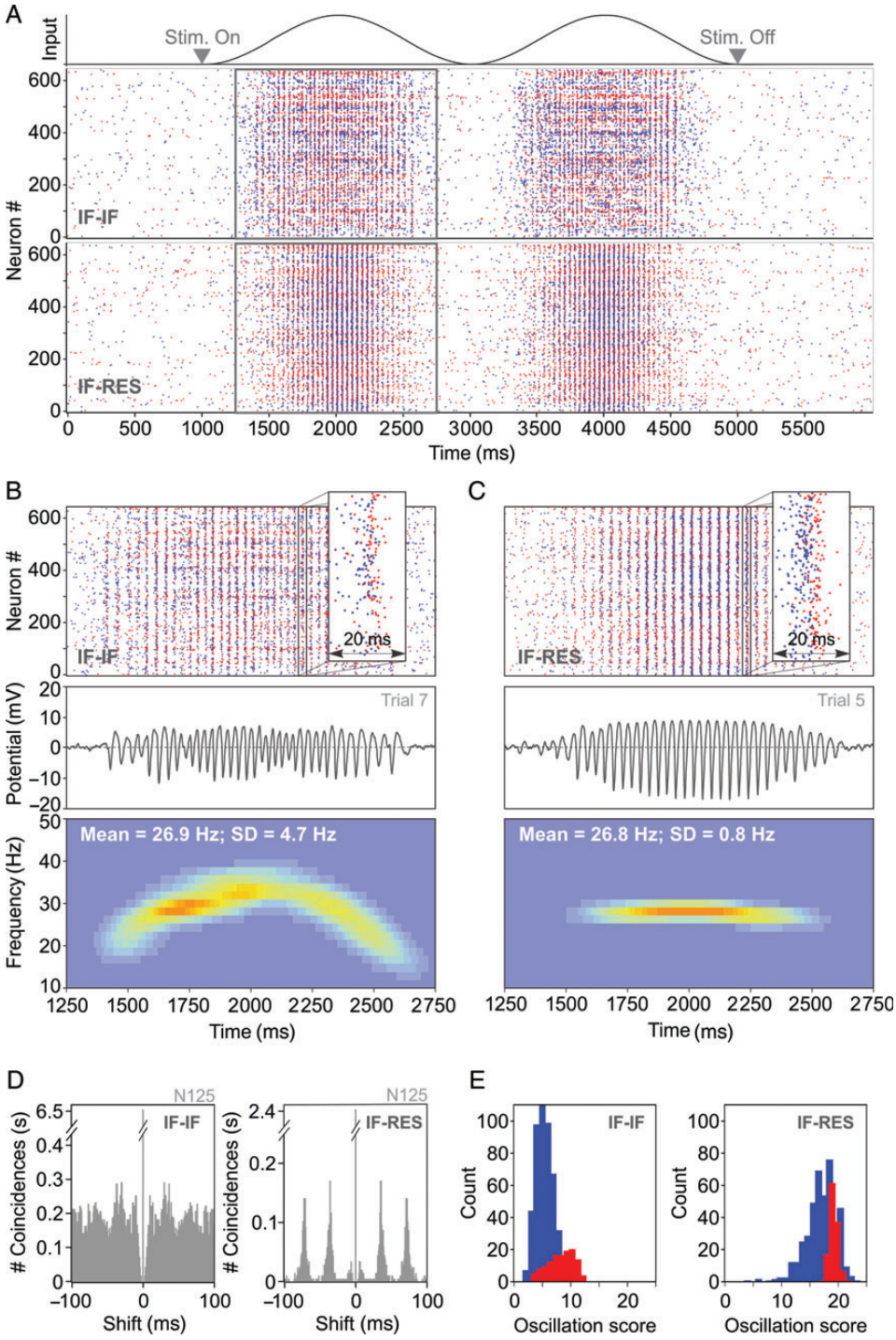

Figure 2. Gamma oscillations in simulated neuronal circuits. (*A*) Input (top) and spike rasters of a single trial activity in integrator–integrator (IF–IF) and integrator–resonator (IF–RES) networks composed of 625 neurons. Rectangles indicate a section of IF–IF and IF–RES activity that is expanded in (*B*) and (*C*), respectively. Spikes are coded in blue for excitatory neurons and in red for inhibitory neurons. (B) Top, zoomed in IF–IF raster from (A); middle, local field potential corresponding to spike raster above; bottom, time-resolved power spectrum of the local field potential averaged across 20 trials. (C) Same as in (B), but corresponding to the IF–RES network from (A). (*D*) ACHs corresponding to the activity of a neuron from the IF–IF (left) and the IF–RES networks (right) shown above. (*E*) OS distribution (in the 20–80 Hz band) for excitatory (blue) and inhibitory (red) neurons in the IF–IF (left) and the IF–RES (right) networks.

IF–IF than in IF–RES networks, and that the oscillation was more regular and stronger in the latter (Supplementary Fig. S5). The time-resolved power spectrum of the LFP, averaged across 20 trials (Fig. 2*B* and *C*, bottom), revealed further that oscillation frequency drifted more strongly in IF–IF (SD = 4.7 Hz) than in IF–RES networks (SD = 0.8 Hz; about 6-fold difference).

The same conclusions were reached when analyzing the firing events of individual cells. ACHs of excitatory neurons' activity indicated that oscillatory modulation was less precise in the case of IF–IF (Fig. 2*D*, left) than in IF–RES networks (Fig. 2*D*, right). The distribution of OS (Mureşan et al. 2008) in the beta/gamma band (20–80 Hz), computed across the

entire population of IF–IF network neurons, revealed low values (most OS values < 10) (Fig. 2*E*, left), indicating a lack of stable oscillatory modulation in the activity of individual cells. By contrast, in IF–RES networks firing patterns of the majority of neurons exhibited strong and stable oscillatory modulation (most OS values > 10) (Fig. 2*E*, right).

Thus, induced gamma oscillations were stronger and more stable when inhibitory interneurons exhibited membrane resonance. In the following analyses, networks presented in Figure 2 were considered to be the reference. Several parameters were subsequently manipulated to understand the parameter and regime dependence of gamma oscillations in the two types of networks.

Parameter Dependence of Emergent Oscillations

Inhibition is critical for the emergence of fast oscillations (Buzsáki et al. 1983; Whittington et al. 2000; Cardin et al. 2009; Sohal et al. 2009) and the timescale of inhibitory currents is known to play a major role in controlling the frequency of the oscillations. Application of barbiturates alters the gating of the $GABA_A$ receptor and prolongs the decay of the inhibitory post-synaptic current (IPSC), leading to a decrease in oscillation frequency (Whittington et al. 1995, 2000; Bartos et al. 2007). We next manipulated the decay time constant of inhibitory synapses (τ_{inh}) and computed, from network LFP, the mean and drift (SD) of oscillation frequency along the stimulus responses. Both types of networks exhibited high oscillation frequency and large frequency drift for very small τ_{inh} (1 ms), indicating that too short IPSCs are not able to counterbalance excitation (Fig. 3*A*). In IF–IF networks, oscillation frequency (Fig. 3*A*, left) and its drift along the stimulus (Fig. 3*A*, right) decreased with increasing τ_{inh}, while in IF–RES networks this decrease ceased for $\tau_{inh} \geq 5$ ms.

Another important factor that influences oscillation frequency is the synaptic conductance delay (Maex and De Schutter 2003). Maximum conductance delays, corresponding to connections among most distant neurons, were next manipulated in a range between 1 and 9 ms (Fig. 3*B*). With increasing delay, there was a monotonic decrease in oscillation frequency for both types of networks (Fig. 3*B*, left). However, while the frequency drift decreased in IF–IF networks as a function of increasing delay, it remained relatively constant, at low levels, in IF–RES networks (Fig. 3*B*, right).

Manipulation of τ_{inh} and conductance delays revealed two important properties of gamma oscillations in the two types of networks. First, in IF–RES networks, the oscillation frequency remained bound within a more narrow band when compared with IF–IF networks (Fig. 3*A*, left, and *B*, left). As will be shown later, this property is due to the frequency preference of inhibitory interneurons in IF–RES networks that keep the oscillation frequency bound within the peak of their resonant input impedance (Supplementary Fig. S3B). Second, in both parameter manipulations, the frequency drift in IF–RES networks was considerably smaller than in IF–IF networks, indicating that the oscillations were always more stable in the former than in the latter.

Networks generating gamma oscillations are relatively complex, with nonlinear dynamics that may be strongly regime-dependent (Brunel and Hakim 1999; Bartos et al. 2007). In addition to synaptic decay and conduction delays, we also manipulated synaptic connectivity strengths that may dramatically influence the operating regime of such networks. Each of the four types of synapses (excitatory–excitatory, excitatory–inhibitory, inhibitory–excitatory, inhibitory–inhibitory) was changed in a range of −20%, 0%, and +20% around the value used in our reference networks, yielding three values for each connectivity strength. We then tested multiple IF–IF and IF–RES networks with all possible combinations of parameter values (81 combinations). The oscillation frequency was broadly influenced by connectivity strength in IF–IF networks around a central frequency of ~28 Hz (Fig. 3*C*, left), while IF–RES networks exhibited oscillation frequencies in a more narrow range of around ~27.5 Hz (Fig. 3*C*, right). For all parameter combinations, the frequency drift was larger in IF–IF networks (drift > 3 Hz; Fig. 3*D*, left) than in IF–RES networks (drift < 3 Hz; Fig. 3*D*, right), indicating that for all connectivity regimes networks with resonator interneurons exhibit more stable gamma oscillations.

Cross-Model Validation and Influence of Resonant Frequency

To check for consistency and model independence of results, we next used a modified RF model (Izhikevich 2001) instead of RES to model interneurons. RF_{fres} neurons exhibit frequency-dependent impedance (Supplementary Fig. S3C) at a frequency of *fres* Hz that can be set explicitly by model parameters (see Materials and Methods). As described for the other networks, reference IF–RF_{20} networks (resonance frequency set to 20 Hz) were first calibrated to obtain firing rates similar to experimental data. Sinusoidal input engaged IF–RF_{20} networks into network oscillations with a frequency of ~31 Hz that was stable along the stimulus (SD = 0.78 Hz) (Supplementary Fig. S6A), reproducing the frequency stability of IF–RES networks.

Unlike in RES neurons, resonant frequency of the RF model can be explicitly set as a parameter and we used this property to test if resonance can "tune" the oscillation frequency of the network. Resonant frequency was systematically varied from 20 to 40 Hz and oscillation frequency and frequency drift were measured in IF–RF networks. Oscillation frequency increased monotonically with the increase in resonant frequency of interneurons, while frequency drift remained at relatively low levels (<1.5 Hz; see Supplementary Fig. S6B). Importantly, similarly to IF–RES, the network oscillation frequency in IF–RF was higher than the central value of the subthreshold resonant impedance peak, e.g., IF–RF_{20} networks oscillated at ~ 31 Hz, and this was a general feature of integrator–resonator networks.

It is unlikely that *in vivo* interneurons in a local population exhibit exactly the same resonant frequency. We therefore studied the behavior of IF–RF networks with heterogeneous resonant frequency. IF–$RF_{20–40}$ networks were set up with individual interneurons having resonant frequencies drawn from a uniform distribution in the range of 20–40 Hz. IF–$RF_{20–40}$ networks exhibited oscillations that were more heterogeneous in frequency, especially when the input was weak (rising and decaying slope of the sinusoidal bump). The frequency became more constrained and less variable at the peak of the input. Importantly, the expected value of the frequency along the stimulus was close to the frequency corresponding to IF–RF_{30} networks (see Supplementary Fig. S6B and S6C). Thus, oscillations in networks with heterogeneous

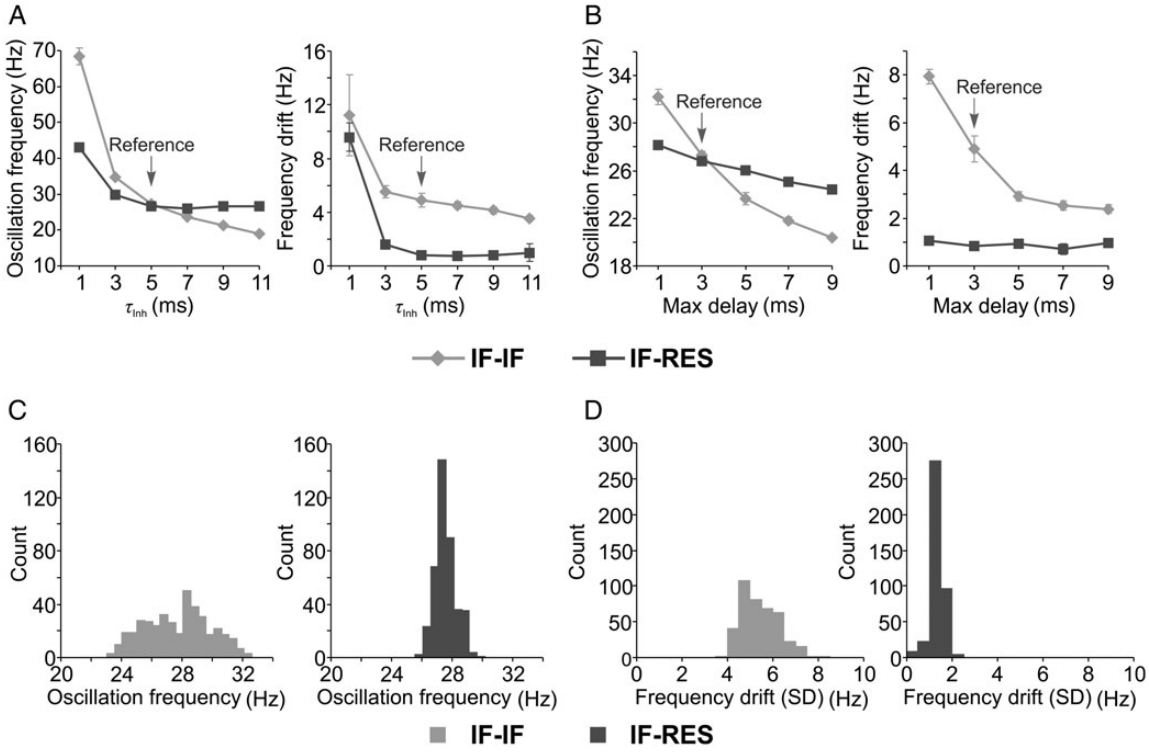

Figure 3. Influence of parameters on gamma oscillations in local circuits. (*A*) Dependence of oscillation frequency (left) and of frequency drift along the stimulus (right) on the decay time constant of inhibitory synapses. (*B*) Dependence of oscillation frequency (left) and of frequency drift along the stimulus (right) on the synaptic conductance delay. (*C* and *D*) Distribution of oscillation frequencies and distributions of frequency drifts along the stimulus, respectively. Distributions were computed for IF–IF (light grey) and IF–RES (dark grey) networks with various synaptic strength combinations. Error bars indicate SD.

resonant frequency exhibit frequencies that are more broadband. These are spread around the frequency generated by a network having interneurons that express the mean of the resonant frequencies. Importantly, the central (mean) oscillation frequency remains stable in time and its variance around the mean decreases with increased input. Strong input reduces the variability of the oscillation frequency and constrains the network more towards its mean oscillation frequency.

Mechanism of Frequency Stability

We next investigated the mechanism that rendered oscillations in IF–RES networks more stable than in IF–IF networks. A first observation is that along a sinusoidal input cycle, neuronal populations were entrained differently in the two types of networks. In IF–IF, the inhibitory population responded only after a corresponding excitatory volley, resulting in balanced population rates whose peaks did not smoothly covary with the sinusoidal input (Fig. 4*A*, left). By contrast, in IF–RES networks and for small values of the input, the inhibitory population exhibited a higher population rate peak per oscillation cycle than the excitatory population, while for strong input this relation reversed. Both population rates were smoothly modulated by the input (Fig. 4*A*, right). The difference stems from the different membrane properties of the inhibitory neurons, as revealed by membrane potential traces (Fig. 4*B*). In IF–IF networks, inhibitory IF neurons responded passively, being purely reactive to the preceding excitatory volley (Fig. 4*B*, top), whereas in IF–RES, inhibitory RES neurons exhibited membrane fluctuations in tandem with the excitatory membrane fluctuations (Fig. 4*B*, bottom, arrows). Cross-correlation functions (CCFs) between average membrane potentials across excitatory and inhibitory populations confirm that in IF–IF networks inhibitory neurons' membranes responded passively to the excitatory entrainment with a delay on the order of ~8–12 ms (Fig. 4*C*, left), while in IF–RES networks the membranes of the two populations fluctuated almost in synchrony (Fig. 4*C*, right). When estimated with a 200-ms long sliding window along the stimulus, the delay between membrane fluctuations changed as a function of the magnitude of network input. In IF–IF, the delay decreased for stronger input, showing that the inhibitory population advanced towards the excitatory population in terms of membrane fluctuations (Fig. 4*D*, left). This relation was opposite for IF–RES networks, the delay being negative for small input and increasing towards positive values for stronger input (Fig. 4*D*, right). These results are at the core to understanding oscillation frequency modulation by input in the studied networks. In IF–IF networks, inhibitory neurons respond passively to excitatory entrainment, a pure PING mechanism, and as a result the oscillation frequency is determined by the recovery period of excitatory neurons from inhibition under the influence of the input—hence the frequency drift, stronger input causing a faster recovery. In IF–RES, inhibitory resonator neurons pace the oscillation cycles by membrane fluctuations that are in synch with those of excitatory neurons. Resonators actively oppose the drift of oscillation frequency: For weak input, excitatory neurons tend to recover from inhibition later than the subthreshold membrane fluctuation of resonators and thus a robust excitatory volley is prevented by the already present, prevailing inhibition

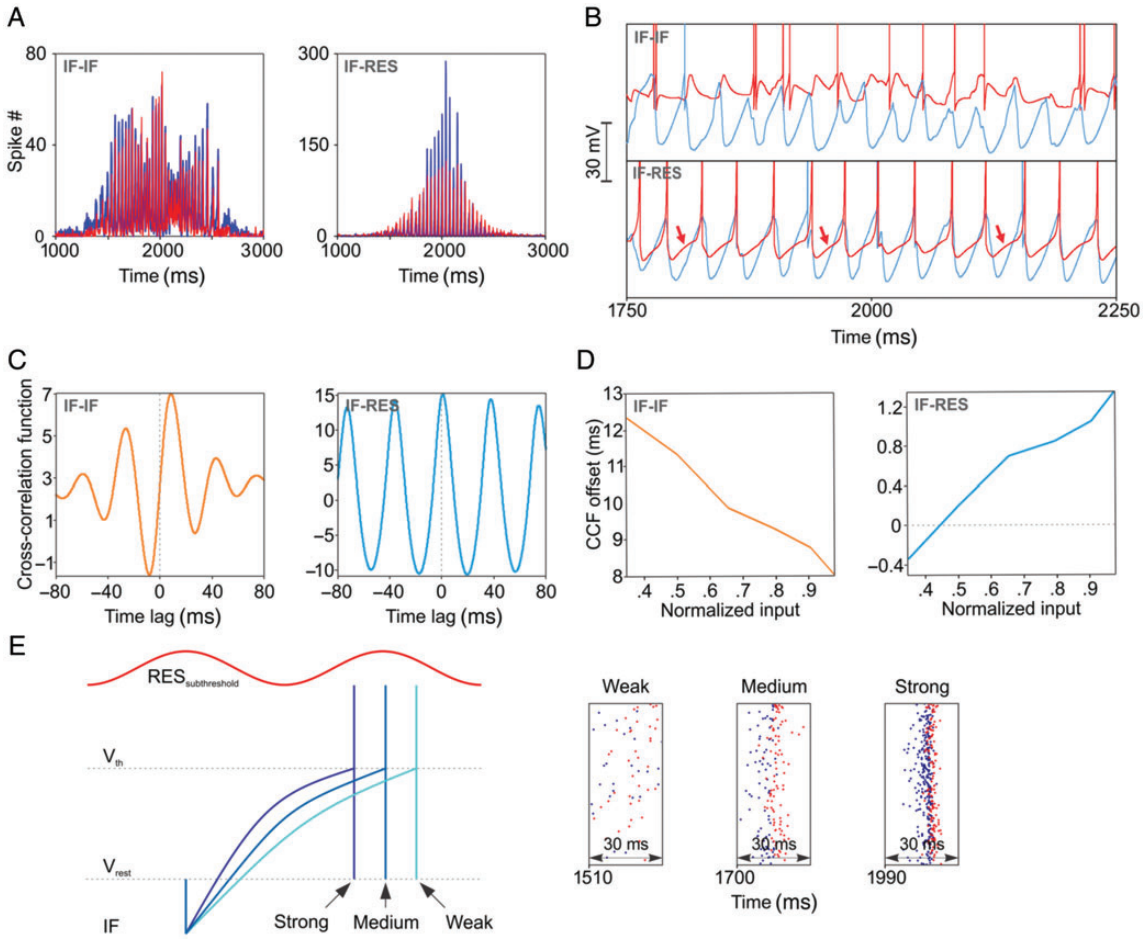

Figure 4. Membrane properties and oscillation mechanisms. (*A*) Population rates of excitatory (blue) and inhibitory (red) neurons. (*B*) Membrane potential trace examples of excitatory (blue) and inhibitory (red) neurons. Arrows indicate the resonant fluctuation of the inhibitory neuron's membrane. (*C*) CCF of average membrane potentials of excitatory and inhibitory populations. (*D*) Offsets of the central peak of CCFs computed with sliding windows of 200 ms along the stimulus (one period of the sinusoid) as a function of the corresponding input to the network. (*E*) Schematic representation of the RING mechanism (left), with example firing sequences in an IF–RES network for different values of the input (right). The blue traces show a schematic firing of the excitatory IF neuron in relation to the subthreshold membrane fluctuation of the inhibitory resonator (red trace) and as a function of input strength.

(Fig. 4*E*; see also right inset with "weak" input where it can be seen that inhibitory neuron spikes are mixed with excitatory neuron spikes). Oscillation cycles longer than the effective resonant period of the interneuron population (in the network, inhibitory–inhibitory coupling of resonators increases the frequency of resonant fluctuations by a few Hz—data shown later) are prevented, the oscillation frequency having thus a lower bound (see also Fig. 3*A*, left, and *C*, right). For strong input, excitatory neurons tend to fire earlier than inhibitory resonators (Fig. 4*E*), which will lag behind and give the excitatory population a larger window of opportunity yielding larger excitatory population rates (Fig. 4*A*, right). The stronger the input the closer and the more synchronously the two populations fire (Fig. 4*E*, right; membrane fluctuations become narrower but their timing relation is as shown in Fig. 4*D*, right). However, inhibitory resonator neurons cannot be advanced too much relative to the effective resonant period such that the resulting IPSCs limit the advancement of excitatory neurons in the next cycle, creating a higher bound on the oscillation frequency. We will call this mechanism RING (Resonance INduced Gamma), and, as we will show later, RING is neither purely PING nor purely ING, but can reproduce both.

To demonstrate that resonance is causally associated with frequency stability, we next manipulated the expression of resonance in interneurons of IF–RES networks. Input impedance at the resonant peak was decreased by increasing the *a* parameter in the Izhikevich model (Izhikevich 2003). As the resonant impedance (*Z*) became smaller, the oscillation frequency decreased (Supplementary Fig. S7A) and the frequency drift increased (Supplementary Fig. S7B). In addition, to check whether the identified RING mechanism is not an artifact due to the different models of interneuron but is indeed relying on membrane resonance, we kept the interneuron model unchanged (i.e. Izhikevich type) but manipulated the parameters of the Izhikevich model from resonator to regular-spiking (RS). We found that the frequency drift was larger in IF–RS than in IF–RES and comparable to that of IF–IF networks, although more stable on the rising front of the input drive (Supplementary Fig. S7C). RS neurons display frequency adaptation (Izhikevich 2003) and fire with higher frequency at the onset of stimulation. Adaptation allowed RS interneurons to entrain to higher initial frequency and to compensate for the smaller initial input, thus stabilizing frequency on the rising slope of the input drive. This further demonstrates the importance of membrane properties of

interneurons in shaping the oscillatory behavior of networks. Finally, membrane potential traces (Supplementary Fig. S7D) and CCFs of average membrane potentials (Supplementary Fig. S7E) revealed that RS interneurons did not display membrane fluctuations in synch with excitatory neurons but were delayed similarly as in IF–IF networks, as predicted by their more integrator-like properties (Mureşan and Savin 2007).

Synchronization, Population Dynamics, and Frequency Stability

Since the dynamics of IPSCs is known to be crucial in determining oscillation frequency (Whittington et al. 2000), we computed the IPSC at the level of the network by averaging across IPSCs recorded in every neuron of IF–IF (Fig. 5*A*, left) and IF–RES (Fig. 5*B*, left) networks. Trough values of network IPSC in each gamma cycle (dots in Fig. 5*A*, left, and *B*, left) were then correlated with the input current (Fig. 5*A*, right, and *B*, right) to estimate how well the inhibition was able to compensate for the change in external drive. To maintain oscillation frequency stable, IPSC troughs should be negatively correlated to the input, i.e. larger negative currents for stronger external excitation. Correlation corresponding to IF–IF networks (mean = – 0.46, SD = 0.1) was significantly poorer ($P < 0.001$, heteroscedastic *t*-test) than correlation in IF–RES networks (mean = – 0.97; SD = 0.0025), indicating that the amplitude of IPSCs faithfully followed the input drive only in the latter (Fig. 5*C*).

At a closer look, we noticed that in IF–IF networks, individual oscillation cycles were frequently "jittered", becoming broader and less precisely synchronized, especially for larger values of the input drive (e.g. Fig. 2*B* top, at around 1750 ms). These desynchronization events appeared stochastically with higher probability when input drive was larger. To quantify such effects, we computed a measure of synchronization across the population of inhibitory neurons, SI (see Materials and Methods). This measure quantifies synchronization across an entire population of neurons, it is independent of firing rate, and takes higher values for stronger synchronization. The average SI across the entire stimulus duration in IF–IF networks (mean = 10.33; SD = 1.11) was significantly lower ($P < 0.001$, heteroscedastic *t*-test) than that corresponding to IF–RES networks (mean = 19.11; SD = 0.33), indicating that, on average, resonator interneurons in IF–RES networks were better synchronized in each gamma cycle than integrator interneurons in IF–IF networks (Fig. 5*D*). The SI was then computed for each individual oscillation cycle and we correlated it to the corresponding input drive (similarly as in Fig. 5*A* and *B*). For IF–IF networks, increased input resulted in less synchronization of interneurons, the two measures being poorly but negatively correlated (Fig. 5*E*; mean = – 0.30; SD = 0.12), confirming the presence of more desynchronized cycles for larger inputs. On the contrary, in IF–RES networks input strength was positively correlated with interneuron synchronization (Fig. 5*E*; mean = 0.85; SD = 0.02). In IF–IF networks, SI of interneurons on each individual gamma cycle was correlated with the duration of the cycle (Fig. 5*F*; mean = 0.57; SD = 0.05), showing that poorer synchronization was associated with a shorter gamma cycle, whereas stronger synchronization was associated with an increased duration of the cycle. The correlation between SI and cycle duration was poor in IF–RES networks (Fig. 5*F*; mean = – 0.32; SD = 0.10) where the duration of the oscillation cycle was comparatively stable along the stimulus.

Occasionally, in certain trials, IF–IF networks had oscillation cycles without desynchronization and in such cases the

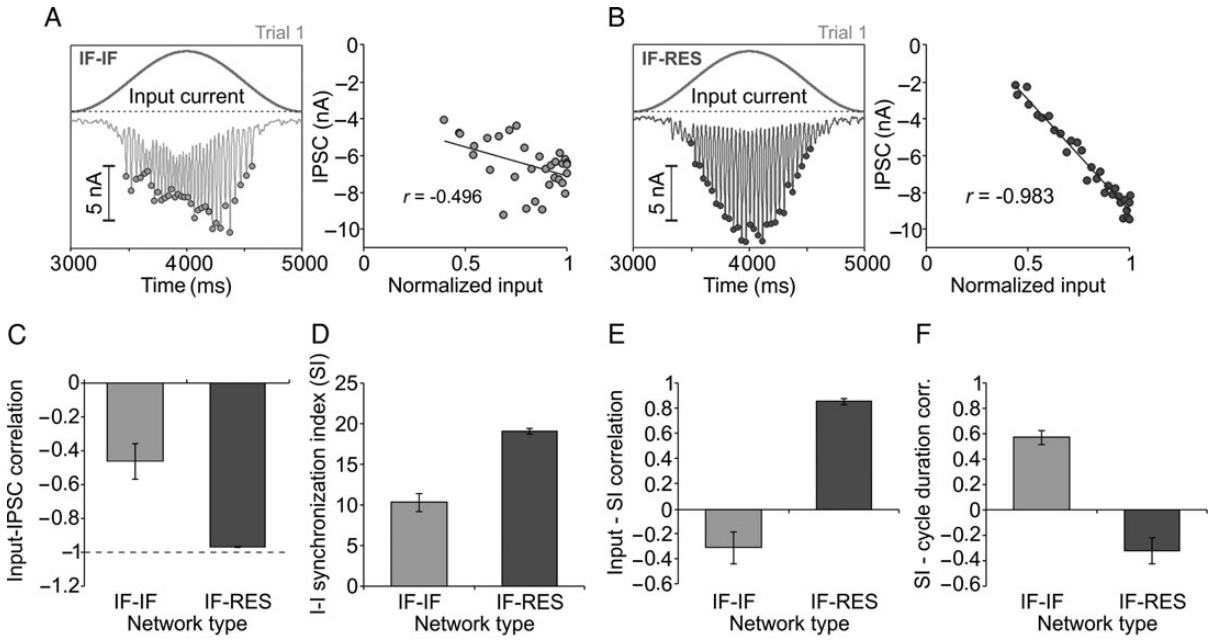

Figure 5. Excitatory/inhibitory population dynamics and frequency stability. (*A*) Analysis of input and inhibitory currents in IF–IF networks. Left, input current and average IPSC across the entire network. Dots indicate troughs of IPSC for each oscillation cycle. Right, IPSC troughs versus normalized input, and their correlation. (*B*) Same as in (A), but for IF–RES networks. (*C*) Correlation between input and IPSC troughs. (*D*) Average SI of inhibitory interneurons over the stimulation period. (*E*) Correlation between instantaneous input and the corresponding SI of inhibitory interneurons at the same moment in time (within the corresponding oscillation cycle). (*F*) Correlation between SI of inhibitory interneurons at the beginning of the oscillation cycle and the duration of the cycle. Error bars indicate SD.

frequency drifts along the stimulus for those trials were smaller than in trials where desynchronization events were observed. For the same activity regime, the lowest drift in IF–IF was nevertheless at least twice as large compared to the largest drift observed in IF–RES networks (data not shown). Thus, RING was always more stable than PING. In addition, desynchronization in PING pushed the frequency drift to even larger values. To investigate why desynchronization events increased frequency drift, we created a simpler setup where inputs were delivered as constant currents to an IF–IF network (input current to: excitatory neurons = 2 nA, inhibitory neurons = 0.3 nA; Fig. 6). Individual inhibitory interneurons received a supplementary strong Gaussian noise with zero mean and SD = 9 nA, for a duration of 4000 ms (Fig. 6*A*), whose effect was to desynchronize them (Fig. 6*B*). Desynchronization was accompanied by a dramatic decrease in the magnitude of IPSCs (Fig. 6*C*, top) and also by a reduction in the firing rates, especially in interneurons (Fig. 6*C*, bottom). During the period with desynchronized cycles, the average oscillation frequency was increased and the power was reduced (Fig. 6*D*). Thus, desynchronization events lead to a dramatic reduction in the amplitude of IPSCs and a concomitant increase in oscillation frequency. Indeed, reduced GABA conductance was shown to advance spiking of principal cells within the cycle in slices of the rat somatosensory cortex (Morita et al. 2008).

The reduction in the IPSC can result from two distinct phenomena. First, poor synchronization leads to poor summation of afferent IPSCs and therefore the resulting IPSC is smaller in amplitude but more spread out in time. We determined that suboptimal summation had only a small effect on the oscillation frequency (Supplementary Fig. S8A). The second possibility is that IPSCs are strongly reduced by the lack of robust firing of afferent interneurons, as suggested by Figure 6*C*, bottom. This effect was evident when we computed population firing rates and compared them to the duration of the corresponding cycle: cycles corresponding to less synchronized epochs, with lower population rates, were shorter than cycles corresponding to more synchronized epochs, with higher population rates (Supplementary Fig. S8B). The spike raster for the IF–IF network in Supplementary Figure S8B also reveals that in well synchronized cycles, a robust synchronous volley of the excitatory population is followed by a strong and synchronous activation of inhibitory neurons, the firing of the latter being clearly delayed. By contrast, in cycles with poor synchronization, interneurons fire also earlier in the cycle and interfere with the development of a robust excitatory volley, this leading in turn to a reduced inhibitory volley. This effect is more likely as the input becomes stronger because membrane fluctuations of IF interneurons advance towards those of excitatory neurons (Fig. 4*D*, left) and the probability of interference is increased. Indeed, we found that in IF–IF networks, increasing the amplitude of external drive to interneurons was accompanied by more frequent desynchronizations and by larger frequency drifts (data shown later). In contrast to IF–IF, in IF–RES networks the resonant property of interneurons keeps them delayed from the excitatory neurons as the input drive increases (Fig. 4*D*, right) and prevents interference that could lead to desynchronization. RING is therefore more robust than purely integrator PING.

Mechanism of synchronization and network oscillation frequency in RING

We further sought to understand why cycle synchronization was more robust in integrator–resonator than in pure integrator networks. Because it is more linear and easier to understand, we first used the RF model of interneuron and applied a slight subthreshold depolarization such as to obtain multiple neurons oscillating at different phases. This mimics a desynchronized interneuron population. When stimulated with a common IPSC corresponding to inhibitory volleys within the cycle, phase delays between different interneurons were dramatically reduced (Fig. 7*A*, top) and this reduction was stronger for larger amplitude IPSC (Fig. 7*A*, bottom). A systematic investigation on RF (Fig. 7*B*, top) and RES (Fig. 7*B*, bottom) models confirmed that phase differences between pairs of neurons were reduced by common IPSCs and that this reduction was stronger for larger amplitude IPSCs. Phase portrait analysis of pairs of delayed RF (Fig. 7*C*) and RES (Fig. 7*D*) interneurons demonstrates that the application of a common IPSC (at the same moment in time) reduces the phase delay between these pairs because the neuron that lags behind is advanced more than the neuron that leads in phase. It is also evident that the larger the amplitude of the IPSC, the smaller the end phase difference (in the limit, if the IPSC tends to $-\infty$, the end phase difference would be 0). Thus, common IPSCs increase synchronization of delayed resonators in a manner proportional to the amplitude of IPSCs.

Unintuitively, network oscillation frequency in integrator–resonator networks was always higher than the subthreshold resonant frequency. This can be explained by noting that embedded in networks resonator neurons change their oscillatory phase dynamics as a function of the input and its timing. Figure 8*A* and *B* depicts the change in oscillatory phase dynamics of RF and RES neurons, respectively, as a function of the type of input (EPSC or IPSC) and phase at which input is received. Effects are qualitatively identical for the two models and are general for any resonator neuron. The phase of a resonator is advanced, i.e. frequency increases, either when the neuron receives an IPSC in the upper semiplane $(0,\pi)$ or an EPSC in the lower semiplane $(-\pi,0)$. By contrast, the phase is delayed, i.e. frequency decreases, when a resonator receives and EPSC in the upper semiplane or an IPSC in the lower semiplane (Fig. 8*A* and *B*). Phase portraits of example RF and RES interneurons (Fig. 8*C* and *D*, respectively) that were embedded in their corresponding IF–RF and IF–RES networks reveal why network oscillation frequency was always higher than the subthreshold resonant frequency. In IF–RF networks, RF neurons received excitation mainly in the lower semiplane and inhibition mainly in the upper semiplane (Fig. 8*C*, top), thus accelerating the phase of the resonator. Delays generated by the amount of excitation preceding or following spikes from the upper semiplane were compensated by positive phase jumps induced by spike resets (Fig. 8*C*, top, arrow). These effects were easily identifiable when the median phase was computed around RF spikes (Fig. 8*C*, bottom). Clearly, the phase dynamics of the network RF neuron was accelerated compared with its isolated subthreshold dynamics. For the case of the RES neuron, the angular phase varies nonlinearly because the phase-portrait deviates significantly from a circle (Fig. 8*D*, top). Nevertheless, similar conclusions can be drawn: starting on the

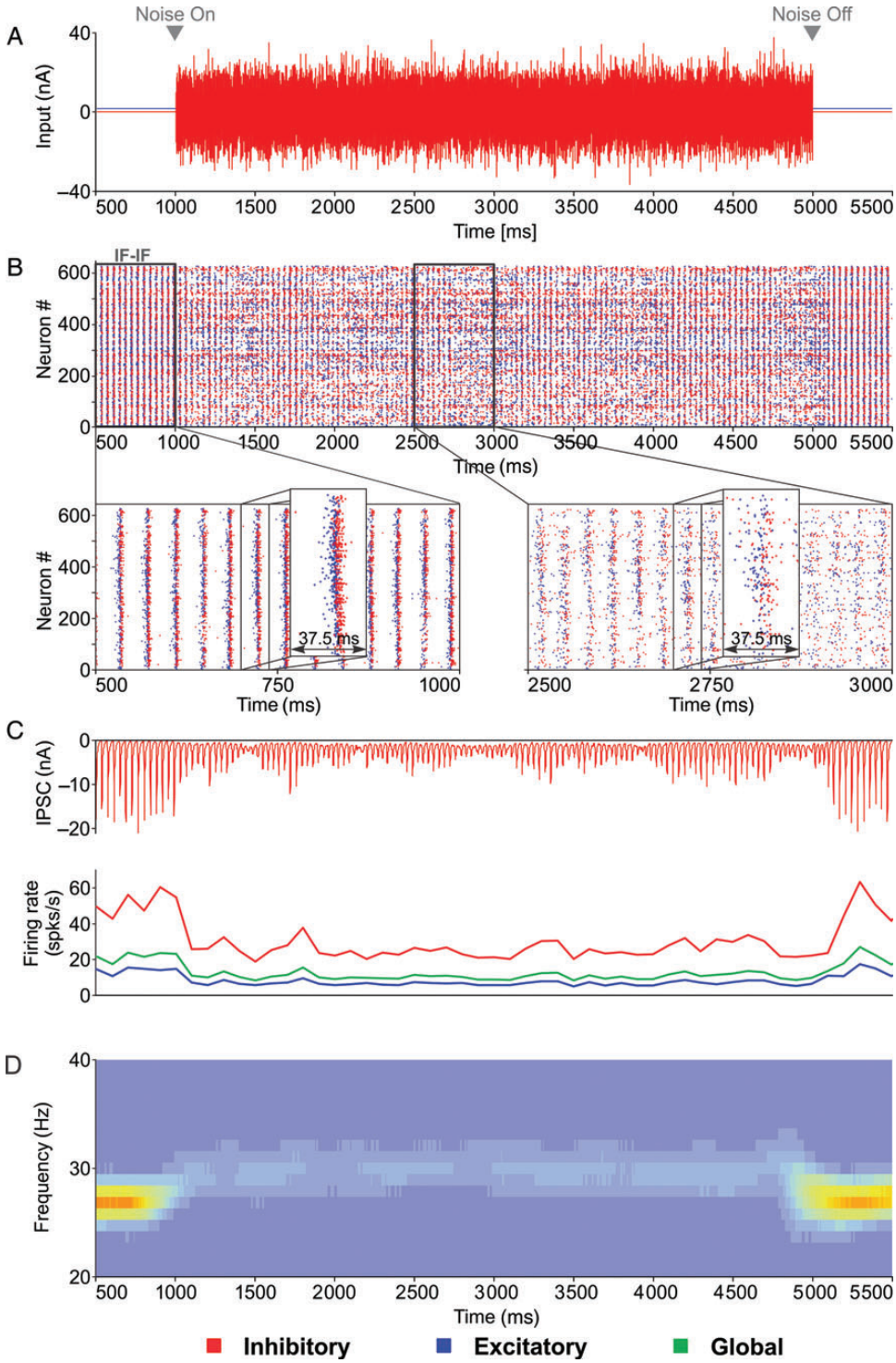

Figure 6. Relationship between interneuron synchronization and oscillation frequency studied in a simplified IF–IF setup. (*A*) Inputs were delivered as constant currents. Between $t = 1000$ and $t = 5000$ ms, a Gaussian noise with zero mean and SD = 9 nA was in addition delivered to interneurons in order to desynchronize them. (*B*) A single trial of an IF–IF network with insets showing a portion of stronger (left) and poorer (right) synchronization. (*C*) Average IPSC across the network and time-resolved firing rates (100 ms window) corresponding to the trial in (*B*). (*D*) Average time-resolved power spectrum computed over 20 trials.

right-hand side of the phase-portrait (Fig. 8*D*, top), RES neurons received first excitation in the upper semiplane (delay) and then inhibition (advance), followed by spike reset that further advanced the phase (Fig. 8*D*, top and bottom). Inhibition following the spike then contributed to a net advancement of the phase, because it hits the neuron mainly in the upper semiplane, accelerating its dynamics (Fig. 8*D*, top).

That inhibition played a crucial role in advancing the phase and the increased frequency of resonators became evident when inhibitory–inhibitory connections were 2×

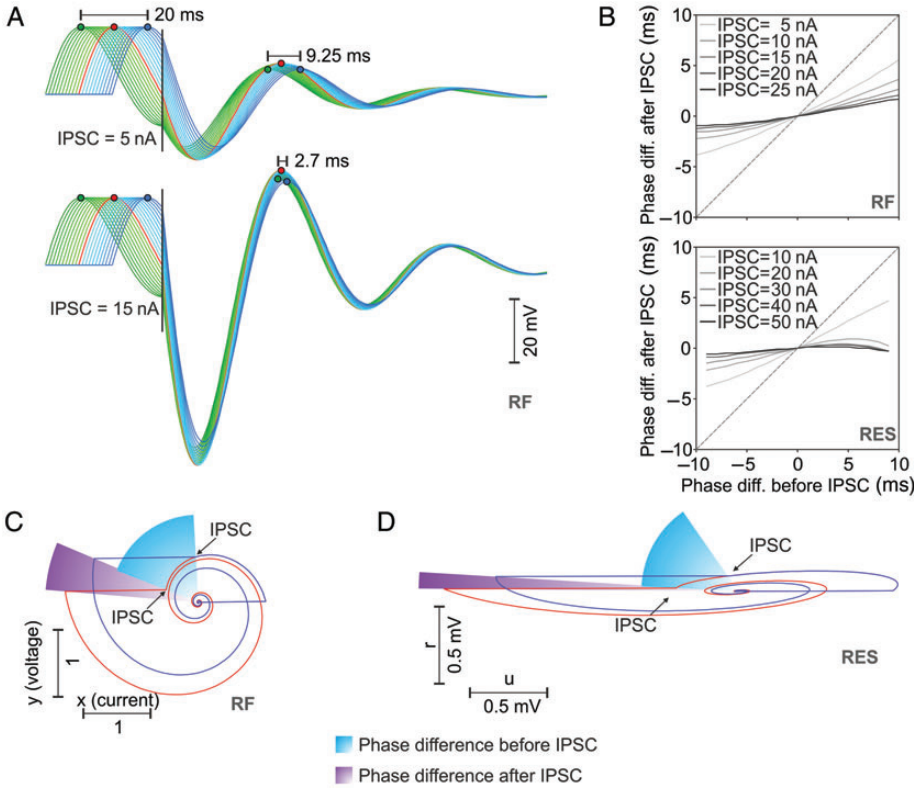

Figure 7. Interneuronal synchronization in integrator–resonator networks. (*A*) Multiple RF interneurons having different phases receive a common IPSC of 5 nA (top) or 15 nA (bottom) that reduce the phase delays. (*B*) Phase difference after IPSC as a function of phase difference before IPSC for pairs of RF (top) or Izhikevich-type resonator (RES; bottom) neurons. Different curves correspond to different amplitudes of the IPSC. (*C*) Phase portrait analysis of two RF neurons with different phases receiving a common IPSC at the same moment in time reveals the mechanism of reduction in phase differences (note that angular velocity is constant for RF neurons). (*D*) Same as in (*C*) but for the case of RES neurons.

strengthened. Figure 8*E*, top, shows, for the same neurons depicted in Figure 8*C* and *D*, that stronger inhibition pushed the excitatory inputs towards the lower semiplane. Furthermore, inhibition was mainly expressed after the spike, because it originated from the network inhibitory volley. The postspike inhibition clearly increased the slope of the phase function (Fig. 8*E*, bottom) thus increasing the frequency of the resonator. In conclusion, the interplay of network excitation and inhibition timed at different phases advances resonator interneurons rendering network oscillation frequency higher than subthreshold resonance frequency of isolated neurons.

Inhibitory Coupling, PING, ING, and RING

Reciprocal inhibitory coupling between interneurons was suggested to have an important role in the development of gamma oscillations (Bartos et al. 2007). To investigate this issue, we considered again networks receiving sinusoidal input and manipulated inhibitory–inhibitory coupling strength by scaling it in a range of 0–2 with respect to the reference (Fig. 9*A*–*C*). When inhibitory neurons were not coupled directly (scaling = 0), networks exhibited oscillations with lower frequency (Fig. 9*A*) and interneurons fired in a more synchronous window for IF–IF networks (Fig. 9*C*). In this case, inhibitory interneurons did not inhibit each other, thus allowing for sharper, more aligned, inhibitory firing. When the strength of reciprocal inhibitory connections was increased, the frequency in both types of networks increased (Fig. 9*A*), while frequency drift increased in IF–IF networks but decreased in IF–RES networks (Fig. 9*B*). Increased reciprocal inhibitory connection strength also led to progressively less synchronized interneurons in IF–IF networks (Fig. 9*C*), indicating that reciprocal inhibition had a desynchronizing effect over IF interneurons. By contrast, in IF–RES networks, interneuron synchronization was always much higher than in IF–IF networks. By increasing inhibitory connectivity strength, the synchrony of resonators first increased and then decreased (Fig. 9*C*) showing that, at least up to a certain value, stronger reciprocal IPSCs synchronize the interneuronal population better, as shown in Figure 7.

While in IF–IF networks, oscillation frequency increases with I–I connectivity strength because of cycle desynchronization, in IF–RES networks frequency increases because of phase advancement due to inhibition (Fig. 8*E*). This conclusion is further supported by the fact that frequency drift increased in IF–IF, while it decreased in IF–RES networks when inhibitory interaction was strengthened (Fig. 9*B*).

To reveal the type of mechanism at work in generating gamma oscillations, we next silenced the excitatory neurons (by removing all their synapses and inputs) and kept only the inhibitory subnetwork active. LFP analysis revealed that IF–IF networks became non-oscillatory, producing only a broadband fluctuation at the network level (Fig. 9*D*, left), while IF–RES networks were able to generate fast oscillations with a frequency of ~26 Hz (Fig. 9*D*, right). These results indicate that gamma oscillations in IF–IF networks relied on a pure PING

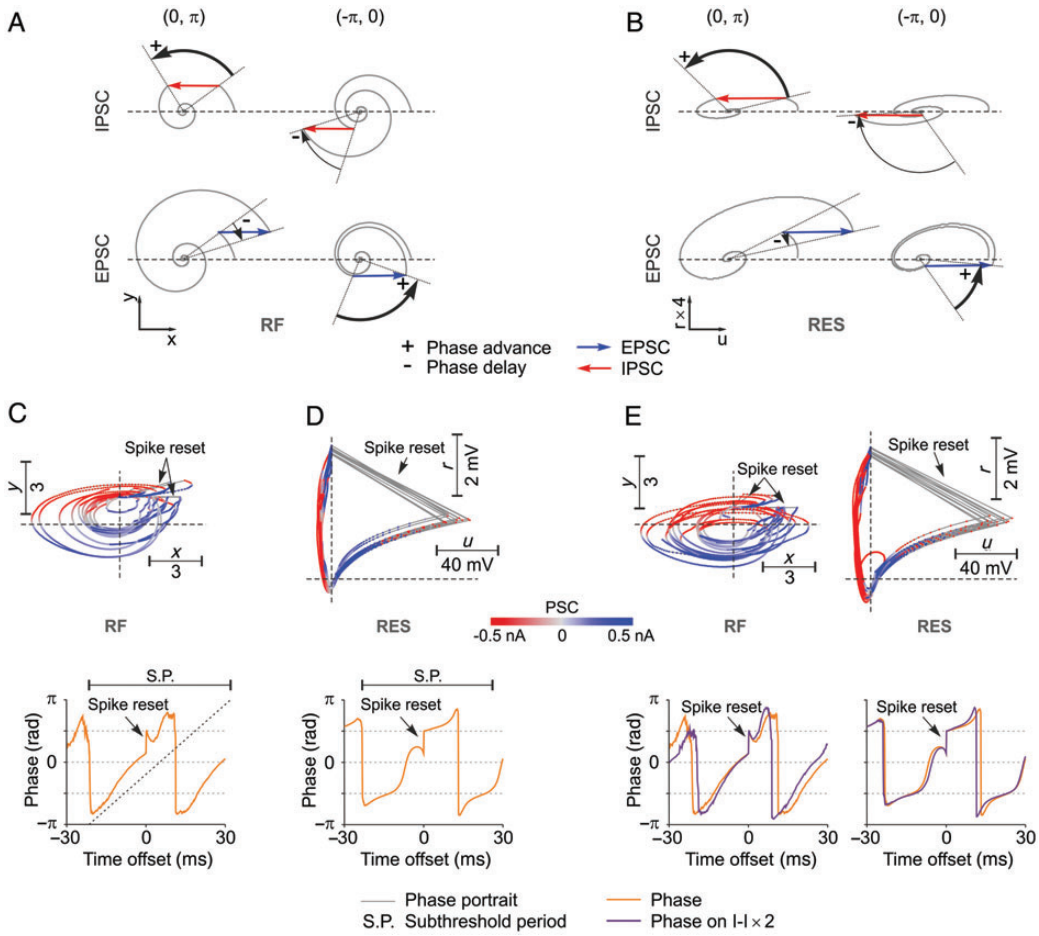

Figure 8. Mechanisms of frequency regulation in RING. (*A*) Phase advancement and delay by IPSC and EPSC as a function of the position of the RF neuron in phase space. (*B*) Same as (*A*) but for the RES neuron. (*C*) Top, phase portrait and the corresponding PSC (color coded) for each position in phase space for an example RF neuron that is part of an IF–RF network. Bottom, median of phases around spikes of the RF neuron (spike-aligned median of phases) computed during the period of oscillatory firing in the network. The segment above depicts the subthreshold resonant period, while the dotted ascending line represents the linear advancement of the phase in the absence of stimulation. (*D*) Same as in (*C*) but for the case of a RES neuron embedded in an IF–RES network. (*E*) Top, phase portraits of the same neurons from (*C*) and (*D*) but with inhibitory–inhibitory connections scaled 2× in the corresponding networks. Bottom, phase dynamics around spikes corresponding to phase portraits above. Phase plots have been overlaid on those from (*C*) and (*D*) for comparison.

mechanism, while isolated subnetworks of resonator interneurons were also able to produce oscillations via an ING-like mechanism. Importantly, synchronization of inhibitory interneurons in IF–RES networks was considerably more robust when excitatory neurons were also active (Fig. 9*E*). Together with evidence of a short time lag between excitatory and inhibitory volleys in IF–RES networks (Fig. 2*C*), our results indicate that RING may reproduce the characteristics of PING when excitatory neurons are active and those of ING when excitatory neurons are silent. Thus, RING is neither purely PING, nor purely ING, but transcends these classifications.

Effect of Input on Oscillatory Activity

We next scaled the amplitude of the sinusoidal inputs and measured the oscillation frequency and its drift in the LFP. Thalamocortical inputs to cortical layer 4 contact both excitatory and inhibitory cells (Thomson and Bannister 2003), and our model respected this anatomy. The scaling was provided to the input of both the excitatory (I_E) and inhibitory (I_I) populations (Fig. 10*A*–*D*). Oscillation frequency was strongly affected by inputs in IF–IF networks, and increased when inputs were scaled up (Fig. 10*A*). Frequency was modulated to a much lesser extent in IF–RES networks (Fig. 10*B*), indicating that in RING the oscillation frequency was kept more bound than in PING. The drift in oscillation frequency was the largest in IF–IF networks, being increased especially when I_I was scaled up (Fig. 10*C*), a scaling that was accompanied by progressively more frequent desynchronization events. By comparison, in IF–RES networks the oscillation frequency was stable across the entire input space, exhibiting only small drifts (Fig. 10*D*).

The timescale of the external input may strongly affect the response properties of brain circuits (Butts et al. 2007). Thus, we manipulated also the temporal properties of the sinusoidal input by changing its frequency over a range of 0.25–64 Hz, yet keeping the amplitude constant. The average LFP power over the gamma band (20–80 Hz) for both IF–IF and IF–RES networks exhibited peaks for input frequencies in the range of 20–30 Hz (Fig. 10*E*), indicating a "resonant circuit property" (Cardin et al. 2009). The two networks are, however, distinguishable by several features (Fig. 10*E*): (i) Peak LFP power was higher in IF–RES networks; (ii) The power peak is

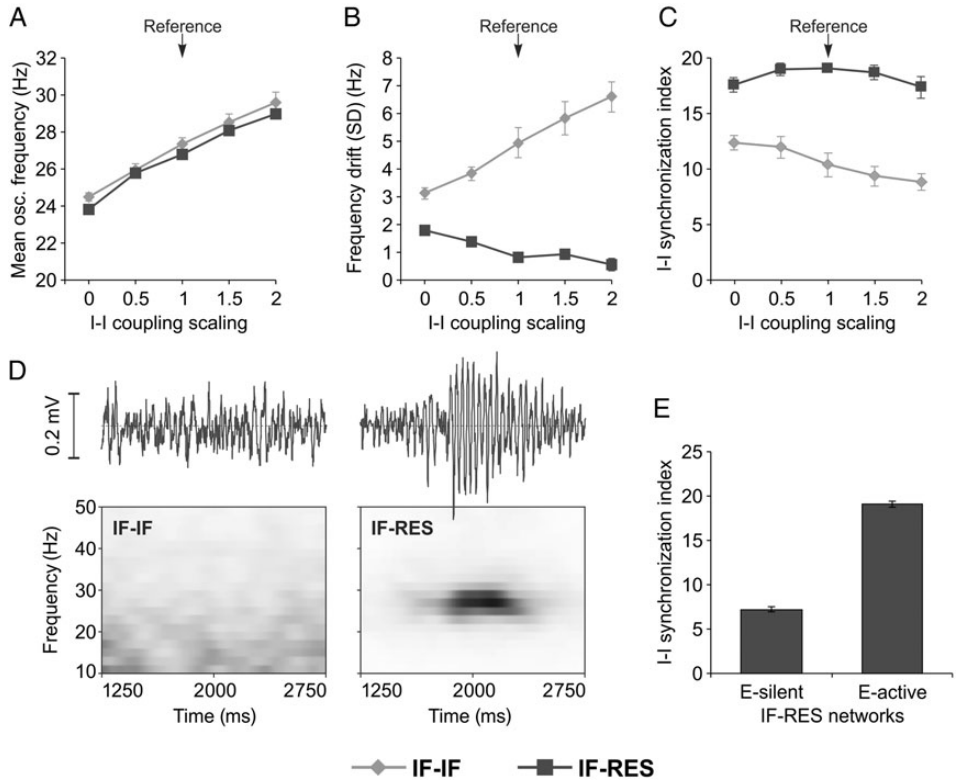

Figure 9. Influence of inhibitory–inhibitory connectivity and oscillation generating mechanisms. (*A*–*C*) Oscillation frequency, frequency drift, and SI of inhibitory interneurons, respectively, as a function of reciprocal connectivity strength between inhibitory interneurons. (*D*) Local field potential (top) and time-resolved power spectrum (bottom) for IF–IF (left) and IF–RES networks (right) with silenced excitatory neurons (corresponding to ING-like mechanism). (*E*) SI of inhibitory interneurons for ING-like RES-only networks (excitatory neurons silent: E-silent) and PING-like IF–RES networks (excitatory neurons active: E-active). Error bars indicate SD.

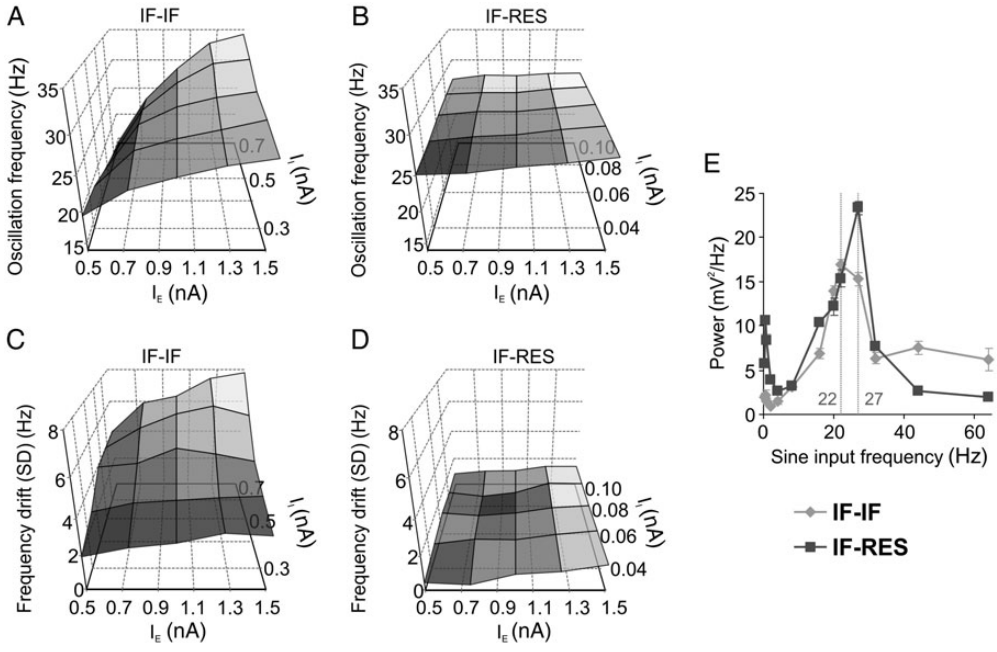

Figure 10. Influence of network inputs on gamma oscillations. (*A* and *B*) Oscillation frequency in IF–IF and IF–RES networks, respectively, as a function of inputs to excitatory (I_E) and inhibitory (I_I) populations. (*C* and *D*) Drift of oscillation frequency along the stimulus in IF–IF and IF–RES networks, respectively, as a function of inputs to excitatory (I_E) and inhibitory (I_I) populations. (*E*) Local field potential power corresponding to the highest peak in the gamma band (20–80 Hz) as a function of frequency of the sinusoidal input. Error bars indicate SD.

more clearly defined for IF–RES networks; (iii) At low input frequencies, IF–RES networks exhibit gamma oscillations with larger power than IF–IF networks; (iv) IF–IF networks are entrained by high frequency input (>30–40 Hz) and exhibit a higher power than IF–RES networks for such inputs.

The input provided to the networks was modeled as a smooth sinusoidal current. *In vivo*, thalamic inputs arrive in the form of afferent spike trains in layer 4. We next tested how networks behaved when input was delivered as spike trains modeled as inhomogeneous Poisson processes whose rates were modulated sinusoidally to a maximum amplitude of 30 spk/s. We found that IF–IF networks were highly sensitive to the decay time constant of excitatory synapses that delivered the input to network neurons (Supplementary Fig. S9A). For small time constants (e.g. 3 ms), IF–IF networks' ability to engage in oscillatory dynamics was strongly impaired, while for large time constants (e.g. 50 ms), these networks behaved more similarly to those receiving a smooth sinusoidal input. IF–RES networks, however, exhibited robust oscillations for all types of inputs, with a somewhat larger frequency drift for small time constants (Supplementary Fig. S9B). These results demonstrate that the oscillatory regime is considerably more robust in IF–RES than in IF–IF networks especially when the external input is noisy (Poisson process). Exactly how noisy the input *in vivo* is difficult to tell, because the smoothness of the input depends not only on the afferent synaptic time constants but also on the total input rate and V1 cells receive their input from multiple LGN afferents (Bruno and Sakmann 2006).

Voltage Dependence of Resonance Frequency

In all investigations, so far resonance frequency was a fixed property for a given interneuron. However, several reports indicate a direct dependency of gamma band resonance frequency on voltage (Fellous et al. 2001; Bracci et al. 2003). Intuitively, an increase in resonance frequency for more depolarized regimes should lead to drift in oscillation frequency of the network due to drift in resonance frequency. Therefore, we next studied the effect of voltage dependence of resonant frequency on network oscillations. The RF model was modified to include a linear, positive dependency of the resonant frequency on the membrane potential and we systematically manipulated the slope of this dependency (Fig. 11*A*, top) in IF–RF networks. As the slope was increased, network oscillations became more robust and network spikes more aligned to the oscillation cycles (Fig. 11*A*, middle rows). Time–frequency plots revealed a decrease of average oscillation frequency and a change from a slightly positive to a slightly negative covariation of network frequency with input (Fig. 11*A*, bottom). Quantitative analyses confirmed that network oscillation frequency decreased as the dependence of resonant frequency on voltage became stronger (larger slope) and that frequency drift remained at relatively low values, <1.5 Hz (Fig. 11*B*).

Thus, a positive dependence of resonance frequency on voltage did not lead to a positive covariation of network oscillation frequency with the strength of the input. This happened because interneurons received strong IPSCs at the end the oscillation cycle which strongly hyperpolarized them between consecutive cycles (Fig. 11*A*, third row)—a period critical for regulation of oscillation frequency. As a result, the tendency of the network was to decrease and not to increase oscillation frequency for strong input because resonators slowed down as their membrane potentials were hyperpolarized in between oscillation cycles. This was also confirmed by analysis of timing relation between membrane fluctuations of excitatory and inhibitory populations: When the slope of the frequency–voltage dependency was larger, the inhibitory resonator neurons tended to lag more behind excitatory neurons (Fig. 11*C*), a phenomenon typical of integrator–resonator networks (see also Fig. 4*D*). This increasing lag gave excitatory neurons a larger window of opportunity, leading to more vigorous excitatory firing followed by more sustained inhibitory firing that produced a decrease in oscillation frequency. Indeed, firing rates increased with the increase in the slope of the frequency–voltage dependency (Fig. 11*D*). Thus, a positive correlation between resonance frequency and membrane potential did not lead to increased network oscillation frequency for stronger input. In contrast, it compensated for such a tendency and even overcompensated for it, leading to decrease in network oscillation frequency for stronger input when the dependence of resonance frequency on membrane voltage was strong.

Discussion

In the cat visual cortex, under anesthesia, induced gamma oscillations can sometimes have remarkably stable oscillation frequency even when the input fluctuates strongly over time. Such stability of frequency is manifested both at the level of individual cells' firing and in LFPs. In the examined data, we have found that frequency was more stable in cases with stronger oscillatory modulation of spiking activity and larger gamma power of the LFP. These findings are complementary to recent results by Ray and Maunsell (2010) showing that in area V1 of awake macaques, gamma oscillation frequency (measured from the LFP) can be strongly modulated by stimulus contrast and co-fluctuates with the latter. The two results may actually be compatible. The large frequency drift as a function of contrast in monkey V1 was accompanied by low gamma power, and in the data analyzed here lower gamma power was also associated to larger frequency drift.

We have also established that the underlying emergence mechanism of observed *in vivo* gamma oscillations in anesthetized cat area 17 resembles PING because narrower action potentials (from putative inhibitory interneurons) follow wider action potentials (of putative pyramidal neurons) across pairs of cells engaged in synchronous oscillations. Time delays between these discharges are small (<5 ms), a finding supported by previous studies in the ferret prefrontal cortex (Hasenstaub et al. 2005) where regular-spiking cells were shown to lead FS interneurons by 4.1 ms, on average. These observations are consistent with a PING-like scenario where inhibitory interneurons are entrained by the excitatory volleys of pyramidal cells (Whittington et al. 2000; Börgers and Kopell 2003).

We have sought to investigate the observed properties of *in vivo* gamma oscillations (frequency stability, power, excitatory–inhibitory firing sequence) by exploring computer models of gamma generator circuits with an emphasis on membrane properties of inhibitory interneurons. The main result of the present study is that membrane resonance expressed in interneurons, as opposed to integration, keeps the

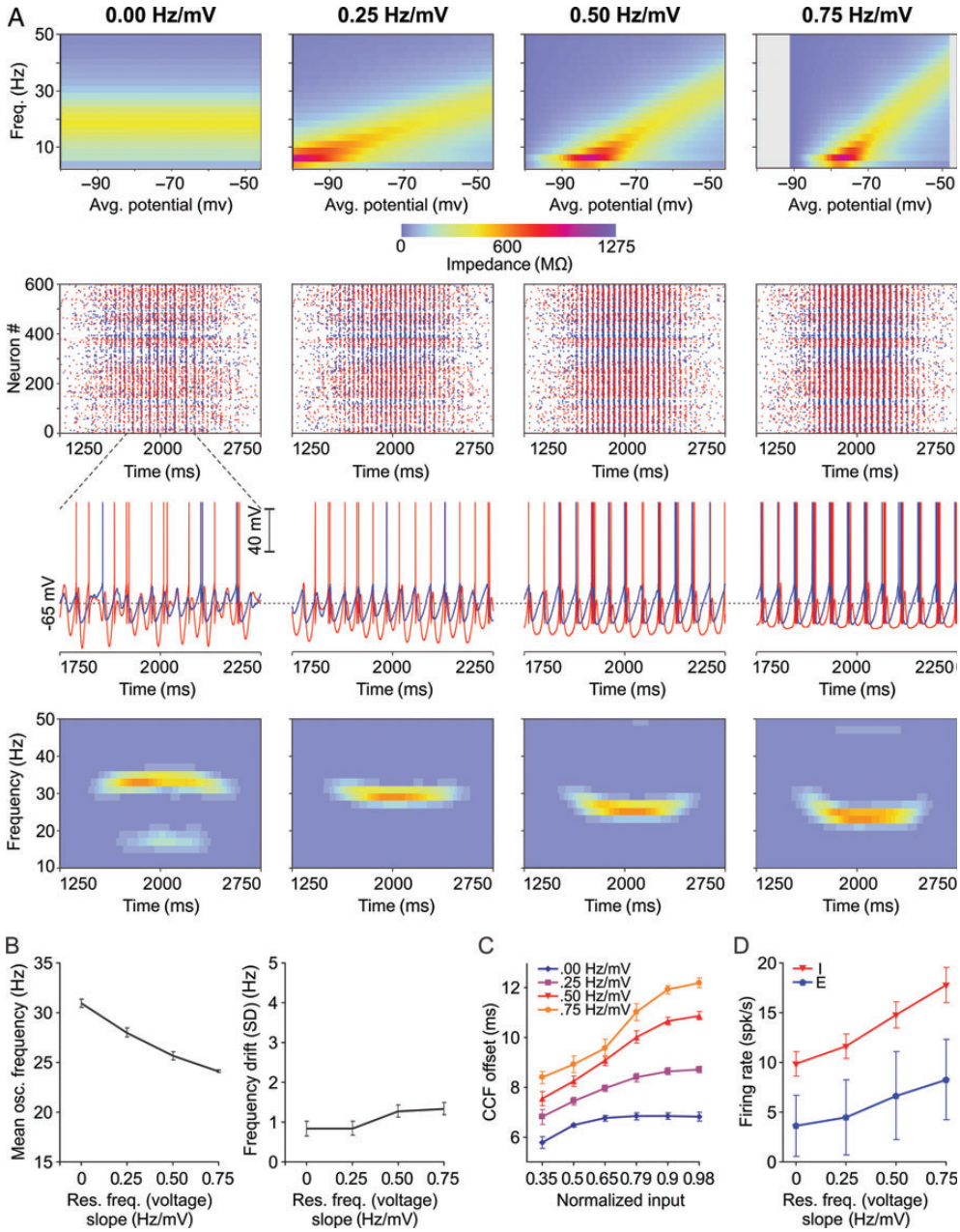

Figure 11. Voltage dependence of resonance frequency. (*A*) Top row: Impedance profiles of a modified RF model neuron whose resonance frequency depends on membrane voltage, with different values of the resonance frequency–voltage slope. Second and third rows: IF–RF network activity during a single sinusoidal input bump and zoom in on membrane potentials of two representative neurons. Each network has RF interneurons with impedance profiles depicted in the corresponding plots above. Bottom row: Time–frequency plots for LFPs generated by the activity of the corresponding networks. (*B*) Mean network oscillation frequency and frequency drift as a function of the frequency–voltage slope impedance characteristic of RF interneurons. (*C*) Offsets of the central peak of CCFs between excitatory and inhibitory membrane fluctuations as a function of normalized amplitude of network input and the slope of the frequency–voltage impedance characteristic of RF interneurons. (*D*) Firing rate of excitatory and inhibitory populations as a function of the slope of the frequency–voltage impedance characteristic of RF interneurons.

oscillation frequency stable and bound within a relatively narrow range, even when time constants of inhibitory synapses (Whittington et al. 1995; Jefferys et al. 1996; Wang and Buzsáki 1996), synaptic conduction delays (Maex and De Schutter 2003), synaptic connection strengths, or magnitudes of the inputs are manipulated. This behavior is enabled by the RING mechanism, whereby the resonant properties of interneurons introduce lower and upper bounds on the period of the oscillation cycle.

Membrane resonance has been suspected to play a role in the development of neuronal oscillations (Llinás et al. 1991; Hutcheon and Yarom 2000; Whittington and Traub 2003; Zemankovics et al. 2010), but it was less clear how and under what conditions. This uncertainty is partly due to the fact that resonance is not a fixed property of neurons but can vary dramatically as a function of several factors. Membrane resonance is voltage-dependent (Gutfreund et al. 1995). *In vitro* studies have shown resonant frequency to be narrow band in some

cases (Llinás et al. 1991), but also tuned up and down by the voltage (Hutcheon et al. 1996). Nevertheless, the shift of resonant frequency in a given cortical state is much smaller than the fluctuation of the firing rate (Amitai 1994; Bracci et al. 2003). In addition, because of its reliance on several voltage-gated ion channels (Hutcheon and Yarom 2000), membrane resonance is expressed differently *in vivo* and *in vitro* (Prescott et al. 2008) and is influenced by several neuromodulators (Steriade et al. 1991; Hutcheon et al. 1996). For example, norepinephrine modulates the hyperpolarization-activated cation current (I_H) and the outwardly rectifying K^+ current (I_K) (Bennett et al. 1986; Banks et al. 1993), while dopamine modulates the persistent sodium current I_{NaP} (Gorelova and Yang 2000) and acetylcholine the M-current (Halliwell and Adams 1982). All these currents are known to contribute to establishment of membrane resonance (Hutcheon and Yarom 2000; Hu et al. 2002; Richardson et al. 2003; Heys et al. 2010). As we have shown here, membrane resonance can greatly enhance stability, robustness, and power of gamma oscillations. Therefore, the regulation of resonance by voltage and neuromodulation in the brain could be a good candidate to explain the dependence of gamma oscillations on cortical state or the variability of experimental results regarding the expression and properties of such oscillations.

Our results further indicate that in purely integrator PING networks, frequency drift can be increased more than expected from the PING mechanism alone due to the interference between the inhibitory and excitatory volleys, which is associated with network desynchronization in individual oscillation cycles. Interference of inhibition with the development of the excitatory volley leads to a cascade effect. The excitatory volley is first reduced, which in turn fails to robustly entrain interneurons such that the resulting IPSCs are considerably smaller. Smaller IPSCs permit a faster recovery from inhibition (Morita et al. 2008), especially as the input to the network increases, leading to a runaway increase in oscillation frequency. That such phenomena observed in our simulated networks are grounded in reality is demonstrated by a recent study of Atallah and Scanziani (2009). They report instantaneous modulation of gamma frequency on a cycle-by-cycle basis in rat hippocampus and show that pyramidal hyperpolarization is longer (longer cycle duration) following a cycle with a larger magnitude of the LFP (and larger IPSCs). This implies, as also shown here, that stronger synchronization (reflected in a larger LFP deflection) is associated with longer cycles, and, conversely, that desynchronization is accompanied by shorter cycles. Thus, a fluctuation of the inhibitory current magnitude, due to population dynamics within each cycle, results in a fluctuation of oscillation frequency. The experimental findings by Atallah and Scanziani (2009) are consistent with the purely integrator IF–IF networks and the mechanisms we have indentified here that lead to frequency drift in such networks. In contrast to PING in purely integrator networks, RING prevents interference of inhibition with the excitatory volley because resonator interneurons do not advance in the oscillation cycle to interfere with the firing of the excitatory population. In addition, synchronization of interneurons is promoted by resonance because, unlike the case of pure integrators, common inhibitory volleys reduce phase delays between resonators. Thus, the synchronous firing of excitatory and inhibitory populations and the timing relation between the two volleys within an oscillation cycle are also crucial in determining the robustness of the oscillation and the stability of oscillation frequency. By the same mechanism, RING also provides robustness of the oscillation when the input is not smooth but noisy.

It is plausible that *in vivo* gamma oscillations in brain circuits are rendered more or less robust by continuous modulation of resonance in interneurons via voltage, neuromodulation, and cortical state changes. When gamma-band resonance in interneurons is expressed stronger, local circuits may exhibit stronger oscillations with a more stable frequency, facilitating their synchronization across large cortical territories. Therefore, modulation of resonance in different brain structures may be instrumental in enabling the development of coherent oscillations and ensuring reciprocal communication channels among different processing modules (Fries 2005; Montgomery and Buzsáki 2007).

The main apparent assumption of the present manuscript is that resonance frequency of interneurons should be fixed to enable frequency stability of network oscillations. But data regarding the *in vivo* resonant properties of fast spiking interneurons in the visual cortex of cats is sparse at best, if not at all missing. Reports in other systems on the dependence of resonant frequency on membrane potential do exist, but results are dependent on the frequency band, the particular neuronal system, the preparation, and so on. Some studies report resonance frequency that increases with depolarization in regular-spiking neurons of the rat somatosensory cortex (Amitai 1994), in striatal FS neurons of rats (Bracci et al. 2003), in guinea-pig cortical neurons (Gutfreund et al. 1995), in thalamic neurons (Puil et al. 1994), and in pyramidal neurons of the olfactory amygdala (Sanhueza and Bacigalupo 2005). Others report that resonance frequency decreases with depolarization in the sensorimotor cortex of juvenile rats (Hutcheon et al. 1996) or in magnocellular neurons of rat supraoptic nucleus (Boehmer et al. 2000). There are also reports of stable resonant frequency that does not depend on membrane voltage in olivary neurons of the guinea pigs (Lampl and Yarom 1997) and stellate cells of the entorhinal cortex (Erchova et al. 2004). Some others describe nonmonotonic dependency of theta-resonance frequency on voltage in pyramidal neurons of CA1 hippocampal area (Hu et al. 2002). Interestingly, Llinás et al. (1991) report in neocortical layer 4 both a voltage dependent resonance in the range of 10–45 Hz and a narrow band 1 around 35–50 Hz that is not dependent on DC current input. In prefrontal cortical slices, Fellous et al. (2001) show that interneurons exhibit two frequency characteristics: a stable resonance frequency at relatively hyperpolarized potentials followed by a positive ramping of resonance frequency for more depolarized potentials. In the absence of exact data for the *in vivo* visual cortex, the most relevant pieces of evidence for our study are those reported for interneurons. Their resonance frequency was shown to be either narrowband and not dependent on voltage (Llinás et al. 1991) or positively correlated to the level of depolarization (Bracci et al. 2003), sometimes for a subregion of the membrane potential domain (Fellous et al. 2001). As we have shown here, in realistic dynamical regimes oscillations are stable in integrator–resonator networks even when resonators exhibit strong positive dependency of resonance frequency on voltage. In fact, because interneurons are hyperpolarized at the end of the oscillation cycle, the covariation of

resonance frequency with voltage leads to a longer resonant cycle (lower frequency) for hyperpolarized potentials. This in turn contributes to a delayed inhibitory response which triggers increased excitatory volleys followed by prolonged inhibition. The stronger the input, the larger the excitatory response which is then followed by more prolonged/increased inhibition which compensates the tendency of the network frequency to increase. If the resonance frequency covaries very strongly with voltage, this can even lead to overcompensation and decreased oscillation frequency for stronger input. Thus, even if its frequency covaries with voltage, resonance enables mechanisms that actively oppose increase in network frequency with increasing input. Moreover, resonant frequency is not expected to vary too much in a realistic regime where membrane potentials do not fluctuate slowly and with large amplitude but rather abruptly and in relatively restricted ranges under heavy network bombardment (Destexhe et al. 2003).

We have found that in networks of integrator neurons, gamma oscillations can be obtained via a PING mechanism. However, in our setup that matched the firing properties of recorded data, we did not manage to obtain ING-like oscillations in networks composed only of inhibitory IF neurons, the presence of excitatory neurons being a prerequisite to obtain network oscillations. This is in apparent contradiction to several other modeling studies that have documented oscillatory activity in purely inhibitory networks with either low (<5 spk/s) (Brunel and Hakim 1999; Brunel and Wang 2003) or high firing rates (>40 Hz) (Wang and Buzsáki 1996; Bartos et al. 2007). In our models, inhibitory interneurons fired in intermediate regimes, rarely exhibiting firing rates of 30–40 Hz, at the peak of the sinusoidal drive. In addition, to mimic realistic *in vivo* conditions, we added miniature synaptic potentials that may have acted to desynchronize the fragile oscillation that appears in isolated inhibitory IF subnetworks. Indeed, it is established that in the absence of some other synaptic mechanisms, such as shunting inhibition (Vida et al. 2006), ING networks composed of integrators are highly sensitive to noise (Wang and Buzsáki 1996; Bartos et al. 2007), the oscillation being quickly disrupted by random fluctuations. Thus, in the firing regime that we have studied, with background miniature release and with fluctuating inputs, networks composed only of integrators generate reliable oscillations only in a PING scenario. By contrast, when interneurons exhibit membrane resonance in the gamma band, oscillations are always robust, regardless of noise or input fluctuations and this holds even when resonance frequency of interneurons is not fixed but spans a relatively large domain. Furthermore, networks of isolated inhibitory resonator neurons are able to generate reliable oscillations similarly to an ING mechanism, but adding excitatory neurons renders oscillations more robust. Our results also indicate that RING is a mechanism that transcends the distinction between ING and PING and can reproduce both. Therefore, networks of integrator-pyramids/resonator-interneurons need to be treated as a special case where the distinction between ING and PING (Whittington et al. 2000; Tiesinga and Sejnowski 2009) may become less relevant.

In purely integrator networks, it was shown that addition of the pyramidal-interneuron loop to an ING network drastically slows down network oscillation when compared with the ING case (Brunel and Wang 2003). By contrast, in RING networks frequency increases by addition of pyramidal-interneuron loops to a subnetwork of resonators and decreases when pyramids are removed or silenced. We have shown that resonator interneurons are accelerated in their phase dynamics (frequency is increased) both by inhibition arriving close to or immediately after the spike and by excitatory volley from pyramids received during the depolarizing phase (lower semiplane of the phase portrait). When excitatory neurons are silenced, resonators are advanced in phase only by inhibition and therefore the oscillation cycle becomes longer, in between the duration of the cycle in the full excitatory–inhibitory network and the natural cycle duration corresponding to the resonant frequency. Thus, the RING mechanism can lead to network properties that are very different from what has been shown for other systems and this further underscores the importance of membrane properties in modulating oscillatory behavior of networks.

The temporal structure of the input is also an important factor determining how gamma oscillations develop. Manipulating the frequency of the sinusoidal input revealed that both IF–IF and IF–RES networks have "resonant circuit property" (Cardin et al. 2009), i.e. LFP power is maximal at stimulation frequencies around a certain characteristic frequency of the network. Thus, circuit resonance can occur also in networks that contain no resonator elements, e.g. IF–IF networks, such that resonance at the level of individual elements should not be confused with resonance at the circuit level. The observed behavior of networks in response to input with various frequencies suggests that network oscillation frequency and circuit resonance are partly hardwired (Bartos et al. 2007), as they emerge from a complex interplay between all network parameters such as membrane time constants, synaptic decay constants, connectivity patterns, resonant frequency of interneurons, and others. Indeed, in integrator–resonator networks, interneuron resonance can coherently determine network oscillation frequency. The latter is always higher than the resonant frequency of interneurons due to phase jumps of resonators under the influence IPSCs or EPSCs received at different phases of the resonant cycle. This mechanism is not at all trivial and is fundamentally different from frequency regulation mechanisms in purely integrator networks. In addition, in networks with heterogeneous resonant frequency of interneurons, multiple individual oscillations coexist and the LFP frequency is dominated by the mean of the network frequencies corresponding to the expressed resonance frequencies.

Manipulation of stimulation frequency further revealed several qualitative differences between the two types of networks we have studied. In purely integrator networks, LFP gamma power was small for low input frequencies but remained relatively large for high input frequencies. By contrast, networks with resonator interneurons exhibited high gamma power for slow inputs and low power for fast inputs. The behavior of these networks resembled that of *in vitro* preparations where gamma oscillations supported by inhibitory subnetworks could be induced with tonic but not with phasic activation (Sohal and Huguenard 2005). It also agrees with *in vivo* findings which suggest that spike-reliability decreases with increasing input frequency (Cardin et al. 2009). Based on these observations, one could analyze extracellularly recorded responses to periodic input (Cardin et al. 2009; Tiesinga and Sejnowski 2009) in order to obtain evidence

either for integrator or resonant behavior of the respective interneuron populations. To further substantiate such investigations, one could also rely on the known frequency-dependent integration of inputs in resonant neurons (Schreiber et al. 2004).

Not only inhibitory interneurons display membrane resonance but several other classes of cells can also exhibit frequency preference, such as the chattering cells (Gray and McCormick 1996) or the fast-rhythmic bursting neurons (Steriade et al. 1998; Cardin et al. 2005). Also, in thalamocortical neurons, dendritic P/Q-type calcium channels support high-frequency membrane potential oscillations in the 20–80 Hz range (Pedroarena and Llinás 1997; Llinás et al. 2007). Here, we have shown that in order to obtain frequency stability of fast oscillations, it is sufficient if resonance is expressed in the inhibitory population and we suggest that the observed frequency preference of FS interneurons (Pike et al. 2000; Fellous et al. 2001; Bracci et al. 2003) can promote robust and stable gamma oscillations. However, it should be investigated also how resonance expressed in excitatory neurons could contribute to gamma oscillations at network level. For other frequency bands, i.e. theta, models of the hippocampal CA3 region predict that theta-band resonance in pyramidal neurons (Leung and Yim 1991; Leung and Yu 1998) contributes to the development of theta oscillations (Tiesinga et al. 2001). With excitatory neurons that resonate in the gamma band, we have previously shown that in randomly connected networks, network-level gamma oscillations appear only transiently (Mureşan and Savin 2007). More recent models suggest that small-world networks composed of resonator–integrator and resonator–resonator populations of excitatory–inhibitory neurons can exhibit frequency stability (Moca and Mureşan 2011), but more research is required to elucidate the detailed mechanisms.

Finally, an important message of the present study is that mechanisms causing the emergence of gamma oscillations are not trivial. Details regarding the interaction between excitatory and inhibitory populations, synchronization within the oscillation cycle, relative phase of firing of pyramids and interneurons, or properties of individual cells can have dramatic effects on both the power and frequency of emergent gamma oscillations. Moreover, the relationship between circuit input and the ensuing gamma rhythms depends strongly on the operation of the particular oscillation-generating mechanism at work. This dependence is not necessarily stationary but can flexibly change as the particular properties of circuit elements and the dynamical states of the circuit change in time. We therefore suggest that there is still much to discover about the functional role and the operation of gamma oscillations in the brain by identifying and understanding the specific oscillation generating mechanisms operating in different subsystems and under different conditions.

Supplementary Material

Supplementary material can be found at: http://www.cercor.oxfordjournals.org/.

Funding

This work was supported by three Romanian grants funded by Ministerul Educaţiei, Cercetării, Tineretului şi Sportului / Unitatea Executivă pentru Finanţarea Învăţământului Superior, a Cercetării, Dezvoltării şi Inovării (UEFISCDI) (grant number PNII-RU-RP-5/2007, contract number 1/01.10.2007, grant number PNII-RU-TE-11/2010, contract number 23/28.07.2010, and grant number PN-II-RU-PD-2011-3-0065/2011, contract number 46/05.10.2011), a "Max Planck–Coneural Partner Group" grant, a Deutsche Forschungsgemeinschaft grant (grant number NI 708/2-1), the Hertie Foundation, the Alexander von Humboldt Stiftung, and the LOEWE Neuronale Koordination Forschungsschwerpunkt Frankfurt (NeFF). Funding to pay the Open Access publication charges for this article was provided by the Hertie Foundation.

Notes

Conflict of Interest: None declared.

References

Amitai Y. 1994. Membrane potential oscillations underlying firing patterns in neocortical neurons. Neuroscience. 63:151–161.

Atallah BV, Scanziani M. 2009. Instantaneous modulation of gamma oscillation frequency by balancing excitation with inhibition. Neuron. 62:566–577.

Banks MI, Pearce RA, Smith PH. 1993. Hyperpolarization-activated cation current (Ih) in neurons of the medial nucleus of the trapezoid body: voltage-clamp analysis and enhancement by norepinephrine and camp suggest a modulatory mechanism in the auditory brain stem. J Neurophysiol. 70:1420–1432.

Bartos M, Vida I, Jonas P. 2007. Synaptic mechanisms of synchronized gamma oscillations in inhibitory interneuron networks. Nat Rev Neurosci. 8:45–56.

Bennett P, McKinney L, Begenisich T, Kass RS. 1986. Adrenergic modulation of the delayed rectifier potassium channel in calf cardiac Purkinje fibers. Biophys J. 49:839–848.

Boehmer G, Greffrath W, Martin E, Hermann S. 2000. Subthreshold oscillation of the membrane potential in magnocellular neurones of the rat supraoptic nucleus. J Physiol. 526(Pt 1):115–128.

Börgers C, Kopell N. 2003. Synchronization in networks of excitatory and inhibitory neurons with sparse, random connectivity. Neural Comput. 15:509–538.

Bracci E, Centonze D, Bernardi G, Calabresi P. 2003. Voltage-dependent membrane potential oscillations of rat striatal fast-spiking interneurons. J Physiol. 549:121–130.

Bragin A, Jandó G, Nádasdy Z, Hetke J, Wise K, Buzsáki G. 1995. Gamma (40–100 Hz) oscillation in the hippocampus of the behaving rat. J Neurosci. 15:47–60.

Brunel N, Hakim V. 1999. Fast global oscillations in networks of integrate-and-fire neurons with low firing rates. Neural Comput. 11:1621–1671.

Brunel N, Wang XJ. 2003. What determines the frequency of fast network oscillations with irregular neural discharges? i. synaptic dynamics and excitation-inhibition balance. J Neurophysiol. 90:415–430.

Bruno RM, Sakmann B. 2006. Cortex is driven by weak but synchronously active thalamocortical synapses. Science. 312:1622–1627.

Buhl EH, Tamás G, Fisahn A. 1998. Cholinergic activation and tonic excitation induce persistent gamma oscillations in mouse somatosensory cortex in vitro. J Physiol. 513(Pt 1):117–126.

Butts DA, Weng C, Jin J, Yeh CI, Lesica NA, Alonso JM, Stanley GB. 2007. Temporal precision in the neural code and the timescales of natural vision. Nature. 449:92–95.

Buzsáki G, Leung LW, Vanderwolf CH. 1983. Cellular bases of hippocampal egg in the behaving rat. Brain Res. 287:139–171.

Buzsáki G, Wang XJ. 2012. Mechanisms of gamma oscillations. Annu Rev Neurosci. 35:203–225.

Cardin JA, Carlén M, Meletis K, Knoblich U, Zhang F, Deisseroth K, Tsai LH, Moore CI. 2009. Driving fast-spiking cells induces gamma rhythm and controls sensory responses. Nature. 459:663–667.
Cardin JA, Palmer LA, Contreras D. 2005. Stimulus-dependent gamma (30–50 Hz) oscillations in simple and complex fast rhythmic bursting cells in primary visual cortex. J Neurosci. 25:5339–5350.
Constantinidis C, Goldman-Rakic PS. 2002. Correlated discharges among putative pyramidal neurons and interneurons in the primate prefrontal cortex. J Neurophysiol. 88:3487–3497.
Destexhe A, Rudolph M, Paré D. 2003. The high-conductance state of neocortical neurons in vivo. Nat Rev Neurosci. 4:739–751.
Erchova I, Kreck G, Heinemann U, Herz AVM. 2004. Dynamics of rat entorhinal cortex layer ii and iii cells: characteristics of membrane potential resonance at rest predict oscillation properties near threshold. J Physiol. 560:89–110.
Fellous JM, Houweling AR, Modi RH, Rao RP, Tiesinga PH, Sejnowski TJ. 2001. Frequency dependence of spike timing reliability in cortical pyramidal cells and interneurons. J Neurophysiol. 85:1782–1787.
Fisahn A, Pike FG, Buhl EH, Paulsen O. 1998. Cholinergic induction of network oscillations at 40 Hz in the hippocampus in vitro. Nature. 394:186–189.
Fries P. 2005. A mechanism for cognitive dynamics: neuronal communication through neuronal coherence. Trends Cogn Sci. 9:474–480.
González-Burgos G, Krimer LS, Povysheva NV, Barrionuevo G, Lewis DA. 2005. Functional properties of fast spiking interneurons and their synaptic connections with pyramidal cells in primate dorsolateral prefrontal cortex. J Neurophysiol. 93:942–953.
Gorelova NA, Yang CR. 2000. Dopamine D1/D5 receptor activation modulates a persistent sodium current in rat prefrontal cortical neurons in vitro. J Neurophysiol. 84:75–87.
Gray CM, Engel AK, König P, Singer W. 1990. Stimulus-dependent neuronal oscillations in cat visual cortex: receptive field properties and feature dependence. Eur J Neurosci. 2:607–619.
Gray CM, McCormick DA. 1996. Chattering cells: superficial pyramidal neurons contributing to the generation of synchronous oscillations in the visual cortex. Science. 274:109–113.
Gray CM, Singer W. 1989. Stimulus-specific neuronal oscillations in orientation columns of cat visual cortex. Proc Natl Acad Sci USA. 86:1698–1702.
Gutfreund Y, Yarom Y, Segev I. 1995. Subthreshold oscillations and resonant frequency in guinea-pig cortical neurons: physiology and modelling. J Physiol. 483(Pt 3):621–640.
Hájos N, Paulsen O. 2009. Network mechanisms of gamma oscillations in the ca3 region of the hippocampus. Neural Netw. 22:1113–1119.
Halliwell JV, Adams PR. 1982. Voltage-clamp analysis of muscarinic excitation in hippocampal neurons. Brain Res. 250:71–92.
Hansel D, Mato G. 2003. Asynchronous states and the emergence of synchrony in large networks of interacting excitatory and inhibitory neurons. Neural Comput. 15:1–56.
Hasenstaub A, Shu Y, Haider B, Kraushaar U, Duque A, McCormick DA. 2005. Inhibitory postsynaptic potentials carry synchronized frequency information in active cortical networks. Neuron. 47:423–435.
Henze DA, Borhegyi Z, Csicsvari J, Mamiya A, Harris KD, Buzsáki G. 2000. Intracellular features predicted by extracellular recordings in the hippocampus in vivo. J Neurophysiol. 84:390–400.
Heys JG, Giocomo LM, Hasselmo ME. 2010. Cholinergic modulation of the resonance properties of stellate cells in layer ii of medial entorhinal cortex. J Neurophysiol. 104:258–270.
Hirsch JA, Gilbert CD. 1991. Synaptic physiology of horizontal connections in the cat's visual cortex. J Neurosci. 11:1800–1809.
Hu H, Vervaeke K, Storm JF. 2002. Two forms of electrical resonance at theta frequencies, generated by M-current, h-current and persistent Na+ current in rat hippocampal pyramidal cells. J Physiol. 545:783–805.
Hubel DH, Wiesel TN. 1962. Receptive fields, binocular interaction and functional architecture in the cat's visual cortex. J Physiol. 160:106–154.
Hutcheon B, Miura RM, Puil E. 1996. Subthreshold membrane resonance in neocortical neurons. J Neurophysiol. 76:683–697.
Hutcheon B, Yarom Y. 2000. Resonance, oscillation and the intrinsic frequency preferences of neurons. Trends Neurosci. 23:216–222.
Izhikevich EM. 2001. Resonate-and-fire neurons. Neural Netw. 14:883–894.
Izhikevich EM. 2003. Simple model of spiking neurons. IEEE Trans Neural Netw. 14:1569–1572.
Izhikevich EM. 2007. Dynamical systems in neuroscience: the geometry of excitability and bursting. Cambridge (MA): MIT Press.
Jefferys JG, Traub RD, Whittington MA. 1996. Neuronal networks for induced '40 Hz' rhythms. Trends Neurosci. 19:202–208.
Krimer LS, Zaitsev AV, Czanner G, Kröner S, González-Burgos G, Povysheva NV, Iyengar S, Barrionuevo G, Lewis DA. 2005. Cluster analysis-based physiological classification and morphological properties of inhibitory neurons in layers 2–3 of monkey dorsolateral prefrontal cortex. J Neurophysiol. 94:3009–3022.
Lampl I, Yarom Y. 1997. Subthreshold oscillations and resonant behavior: two manifestations of the same mechanism. Neuroscience. 78:325–341.
Leung LS, Yu HW. 1998. Theta-frequency resonance in hippocampal ca1 neurons in vitro demonstrated by sinusoidal current injection. J Neurophysiol. 79:1592–1596.
Leung LW, Yim CY. 1991. Intrinsic membrane potential oscillations in hippocampal neurons in vitro. Brain Res. 553:261–274.
Lima B, Singer W, Neuenschwander S. 2011. Gamma responses correlate with temporal expectation in monkey primary visual cortex. J Neurosci. 31:15919–15931.
Lin JW, Faber DS. 2002. Modulation of synaptic delay during synaptic plasticity. Trends Neurosci. 25:449–455.
Llinás RR, Choi S, Urbano FJ, Shin HS. 2007. Gamma-band deficiency and abnormal thalamocortical activity in p/q-type channel mutant mice. Proc Natl Acad Sci USA. 104:17819–17824.
Llinás RR, Grace AA, Yarom Y. 1991. In vitro neurons in mammalian cortical layer 4 exhibit intrinsic oscillatory activity in the 10- to 50-Hz frequency range. Proc Natl Acad Sci USA. 88:897–901.
Maex R, De Schutter E. 2003. Resonant synchronization in heterogeneous networks of inhibitory neurons. J Neurosci. 23:10503–10514.
Melloni L, Molina C, Pena M, Torres D, Singer W, Rodriguez E. 2007. Synchronization of neural activity across cortical areas correlates with conscious perception. J Neurosci. 27:2858–2865.
Mitchell JF, Sundberg KA, Reynolds JH. 2007. Differential attention-dependent response modulation across cell classes in macaque visual area v4. Neuron. 55:131–141.
Moca VV, Mureşan RC. 2011. Emergence of beta/gamma oscillations: ING, PING, and what about RING?. BMC Neuroscience. 12(Suppl. 1):P230.
Montgomery SM, Buzsáki G. 2007. Gamma oscillations dynamically couple hippocampal ca3 and ca1 regions during memory task performance. Proc Natl Acad Sci USA. 104:14495–14500.
Morita K, Kalra R, Aihara K, Robinson HPC. 2008. Recurrent synaptic input and the timing of gamma-frequency-modulated firing of pyramidal cells during neocortical "up" states. J Neurosci. 28:1871–1881.
Mureşan RC, Ignat I. 2004. The "Neocortex" neural simulator. A modern design. Proceedings of International Conference on Intelligent Engineering Systems. Cluj-Napoca, Romania.
Mureşan RC, Jurjuţ OF, Moca VV, Singer W, Nikolić D. 2008. The oscillation score: an efficient method for estimating oscillation strength in neuronal activity. J Neurophysiol. 99:1333–1353.
Mureşan RC, Savin C. 2007. Resonance or integration? Self-sustained dynamics and excitability of neural microcircuits. J Neurophysiol. 97:1911–1930.
Nikolić D. 2009. Model this! Seven empirical phenomena missing in the models of cortical oscillatory dynamics. Proceedings of International Joint Conference on Neural Networks. p 2272–2279.
Olshausen BA, Field DJ. 2006. 23 Problems in Systems Neuroscience, chapter What Is the Other 85 Percent of V1 Doing? Oxford University Press, Inc. p. 182–213.

Paré D, Lebel E, Lang EJ. 1997. Differential impact of miniature synaptic potentials on the soma and dendrites of pyramidal neurons in vivo. J Neurophysiol. 78:1735–1739.
Paré D, Shink E, Gaudreau H, Destexhe A, Lang EJ. 1998. Impact of spontaneous synaptic activity on the resting properties of cat neocortical pyramidal neurons in vivo. J Neurophysiol. 79:1450–1460.
Pedroarena C, Llinás R. 1997. Dendritic calcium conductances generate high-frequency oscillation in thalamocortical neurons. Proc Natl Acad Sci USA. 94:724–728.
Pike FG, Goddard RS, Suckling JM, Ganter P, Kasthuri N, Paulsen O. 2000. Distinct frequency preferences of different types of rat hippocampal neurones in response to oscillatory input currents. J Physiol. 529:205–213.
Prescott SA, Ratté S, Koninck YD, Sejnowski TJ. 2008. Pyramidal neurons switch from integrators in vitro to resonators under in vivo-like conditions. J Neurophysiol. 100:3030–3042.
Puil E, Meiri H, Yarom Y. 1994. Resonant behavior and frequency preferences of thalamic neurons. J Neurophysiol. 71:575–582.
Ray S, Maunsell JHR. 2010. Differences in gamma frequencies across visual cortex restrict their possible use in computation. Neuron. 67:885–896.
Richardson MJE, Brunel N, Hakim V. 2003. From subthreshold to firing-rate resonance. J Neurophysiol. 89:2538–2554.
Sabatini BL, Regehr WG. 1999. Timing of synaptic transmission. Annu Rev Physiol. 61:521–542.
Sanhueza M, Bacigalupo J. 2005. Intrinsic subthreshold oscillations of the membrane potential in pyramidal neurons of the olfactory amygdala. Eur J Neurosci. 22:1618–1626.
Schoffelen JM, Oostenveld R, Fries P. 2005. Neuronal coherence as a mechanism of effective corticospinal interaction. Science. 308:111–113.
Schreiber S, Erchova I, Heinemann U, Herz AVM. 2004. Subthreshold resonance explains the frequency-dependent integration of periodic as well as random stimuli in the entorhinal cortex. J Neurophysiol. 92:408–415.
Singer W. 1999. Neuronal synchrony: a versatile code for the definition of relations?. Neuron. 24:49–65, 111–125.
Sirota A, Montgomery S, Fujisawa S, Isomura Y, Zugaro M, Buzsáki G. 2008. Entrainment of neocortical neurons and gamma oscillations by the hippocampal theta rhythm. Neuron. 60:683–697.
Sohal VS, Huguenard JR. 2005. Inhibitory coupling specifically generates emergent gamma oscillations in diverse cell types. Proc Natl Acad Sci USA. 102:18638–18643.
Sohal VS, Zhang F, Yizhar O, Deisseroth K. 2009. Parvalbumin neurons and gamma rhythms enhance cortical circuit performance. Nature. 459:698–702.
Sporns O, Chialvo DR, Kaiser M, Hilgetag CC. 2004. Organization, development and function of complex brain networks. Trends Cogn Sci. 8:418–425.
Steriade M. 2006. Grouping of brain rhythms in corticothalamic systems. Neuroscience. 137:1087–1106.
Steriade M, Dossi RC, Paré D, Oakson G. 1991. Fast oscillations (20–40 Hz) in thalamocortical systems and their potentiation by mesopontine cholinergic nuclei in the cat. Proc Natl Acad Sci USA. 88:4396–4400.
Steriade M, Timofeev I, Dürmüller N, Grenier F. 1998. Dynamic properties of corticothalamic neurons and local cortical interneurons generating fast rhythmic (30–40 Hz) spike bursts. J Neurophysiol. 79:483–490.
Tallon-Baudry C, Bertrand O, Delpuech C, Permier J. 1997. Oscillatory gamma-band (30–70 Hz) activity induced by a visual search task in humans. J Neurosci. 17:722–734.
Thomson AM, Bannister AP. 2003. Interlaminar connections in the neocortex. Cereb Cortex. 13:5–14.
Tiesinga P, Sejnowski TJ. 2009. Cortical enlightenment: are attentional gamma oscillations driven by ing or ping?. Neuron. 63:727–732.
Tiesinga PH, Fellous JM, José JV, Sejnowski TJ. 2001. Computational model of carbachol-induced delta, theta, and gamma oscillations in the hippocampus. Hippocampus. 11:251–274.
Uhlhaas PJ, Singer W. 2006. Neural synchrony in brain disorders: relevance for cognitive dysfunctions and pathophysiology. Neuron. 52:155–168.
Vida I, Bartos M, Jonas P. 2006. Shunting inhibition improves robustness of gamma oscillations in hippocampal interneuron networks by homogenizing firing rates. Neuron. 49:107–117.
Wang XJ, Buzsáki G. 1996. Gamma oscillation by synaptic inhibition in a hippocampal interneuronal network model. J Neurosci. 16:6402–6413.
Whittington MA, Traub RD. 2003. Interneuron diversity series: inhibitory interneurons and network oscillations in vitro. Trends Neurosci. 26:676–682.
Whittington MA, Traub RD, Jefferys JG. 1995. Synchronized oscillations in interneuron networks driven by metabotropic glutamate receptor activation. Nature. 373:612–615.
Whittington MA, Traub RD, Kopell N, Ermentrout B, Buhl EH. 2000. Inhibition-based rhythms: experimental and mathematical observations on network dynamics. Int J Psychophysiol. 38:315–336.
Yu S, Huang D, Singer W, Nikolic D. 2008. A small world of neuronal synchrony. Cereb Cortex. 18:2891–2901.
Zemankovics R, Káli S, Paulsen O, Freund TF, Hájos N. 2010. Differences in subthreshold resonance of hippocampal pyramidal cells and interneurons: the role of h-current and passive membrane characteristics. J Physiol. 588:2109–2132.